NASA TN D-378

TECHNICAL NOTE

D-378

FORCE INVESTIGATION OF THREE

SURFACE-PIERCING SUPERCAVITATING HYDROFOILS

WITH 45° NEGATIVE DIHEDRAL

By Irving Weinstein

Langley Research Center
Langley Field, Va.

NATIONAL AERONAUTICS AND SPACE ADMINISTRATION

WASHINGTON

June 1960

NATIONAL AERONAUTICS AND SPACE ADMINISTRATION

TECHNICAL NOTE D-378

FORCE INVESTIGATION OF THREE SURFACE-PIERCING SUPERCAVITATING HYDROFOILS WITH 45° NEGATIVE DIHEDRAL

By Irving Weinstein

SUMMARY

An investigation has been made in Langley tank no. 1 to determine the lift, drag, and pitching-moment characteristics of three surface-piercing, supercavitating hydrofoils. The models were two triangular hydrofoils, with and without leading-edge sweep, and a rectangular hydrofoil, each with 45° negative dihedral. The hydrofoils had circular-arc sections with a chamfered upper-surface leading edge having a 2° included angle. These sections are fairly easy to construct and they maintain characteristics of a sharp-leading-edge supercavitating section. Data were obtained at hydrofoil angles of attack up to 20°, speeds up to 70 fps, and depths varying to 1.2 chords.

The data indicate that complete ventilation occurred at angles of attack of 11° and higher for the triangular hydrofoil with leading-edge sweep, at angles of 10° and higher for the triangular hydrofoil without leading-edge sweep, and at angles of 12° and higher for the rectangular hydrofoil. A comparison of the two triangular hydrofoils, which had equal aspect ratios regardless of depth, shows that the one with leading-edge sweep had higher lift-drag ratios. The maximum lift-drag ratios obtained with this hydrofoil were 5.3 in the low-angle partially ventilated region and 4.0 in the fully ventilated region at a depth-chord ratio of 0.8. No abrupt change in lift or drag occurred with an increase in angle of attack from the low angles to the high angles at which the hydrofoils became fully ventilated. In the region of complete ventilation, the lift coefficient increased linearly with increase in angle of attack for all three hydrofoils. A brief comparison shows the experimental data to be in good agreement with that predicted by theory.

INTRODUCTION

Attempts to use the hydrofoil as landing gear for water-based aircraft have generally been hampered by longitudinal instability which

is attributable largely to abrupt changes in lift and drag which occur when the upper surface becomes ventilated or cavitated. The use of a section with a sharp leading edge to induce separation of flow from the upper surface at low speeds alleviates these problems (refs. 1 and 2), although with some decrease in lift-drag ratio.

The sharp-leading-edge, or supercavitating, hydrofoils of the present investigation were of interest as possible landing gear for high-speed aircraft operating on the water at speeds in excess of those at which cavitation can be avoided on conventional thin hydrofoils. Negative dihedral was employed to combine the functions of lifting surface and strut, and to provide reduction of hydrofoil area at high speeds. Hydrofoils of triangular plan form, with and without leading-edge sweep, and a rectangular hydrofoil are included in the investigation. The overall aspect ratio of the hydrofoils is considered to be small enough to be structurally feasible.

Data were obtained from a force investigation made in Langley tank no. 1 to determine the lift, drag, and pitching-moment characteristics of the three surface-piercing supercavitating hydrofoils at 45° negative dihedral. The hydrofoils have circular-arc sections with a leading-edge upper-surface chamfer having a 2° included angle. These sections are fairly easy to construct and they maintain characteristics of a supercavitating section similar to those described in references 1 and 2.

Although data in the region of full ventilation are of primary interest, data also are presented for the nonventilated and partially ventilated conditions. Data were obtained at hydrofoil angles up to 20°, speeds up to 70 feet per second, and depths varying to 1.2 mean geometric chords.

SYMBOLS

b	average projected wetted span, ft
c	mean geometric chord of hydrofoil, 0.30 ft for each model
D	total drag (Air drag + Water resistance), lb
d	depth of tip at trailing edge (measured vertically from undisturbed water surface), ft
L	lift or vertical load, lb
M	pitching moment about trailing edge of hydrofoil at the tip, ft-lb

p_c pressure within cavity, lb/sq ft

p_o pressure at mean depth of hydrofoil, lb/sq ft

q free-stream dynamic pressure, $\frac{1}{2}\rho V^2$

S projected wetted area on undersurface of model, excluding spray wetting, sq ft

V horizontal velocity, fps

C_D drag coefficient, D/qS

C_L lift coefficient, L/qS

$C_{L,d}$ two-dimensional design lift coefficient at infinite depth when the reference line in the plane of the hydrofoil is at zero angle of attack $\frac{\pi}{2}\frac{9}{16}\gamma$ (ref. 2)

C_m moment coefficient about trailing edge at the tip, M/qSc

α angle of attack measured in vertical plane between the horizontal and a line through the leading edge and lower surface of the trailing edge, deg

ρ mass density of water, 1.97 slugs/cu ft for these tests

γ central angle subtending chord of the lower surface of the circular-arc hydrofoil, radians unless otherwise indicated

σ cavitation number, $\frac{p_o - p_c}{q}$

DESCRIPTION OF MODELS

A drawing showing the hydrofoil on the support system is presented as figure 1. The negative dihedral of 45° was chosen for the hydrofoil to give depth stability, and a large root was used to minimize bending stresses. The dihedral angle was measured between the horizontal and the trailing edge of the rectangular or swept-leading-edge triangular model when the mounting plate was horizontal. The dihedral angle was referred to the leading edge for the unswept-leading-edge triangular hydrofoil. The desired angle of attack was obtained by rotating the

system about a lateral pivot axis. A symmetrical system of two hydrofoils was used for the tests to avoid rolling moments and to simulate the spacing that would be used in a practicable application of negative dihedral hydrofoils on the fuselage of a water-based configuration. A few runs with more than three times the basic spacing indicated that there was no appreciable interference effect between the hydrofoils with the basic spacing.

The plan forms of the three hydrofoils tested are presented in figure 2 along with typical cross sections. The test models were made of mild steel and were cadmium plated. The bottom surface was then copper plated in alternate $\frac{1}{2}$-inch strips and darkened with hydrogen sulfide gas. The resulting scale facilitated measurements of the wetted areas from underwater photographs.

The models included a triangular hydrofoil with leading-edge sweep, a triangular hydrofoil without leading-edge sweep, and a rectangular hydrofoil. For simplicity, these hydrofoils may be referred to as model S (swept triangular), model U (unswept triangular), and model R (rectangular). All the hydrofoils had circular-arc cross sections for ease of construction. They were made by bending a $\frac{3}{32}$-inch plate until each section had the desired central angle of 16° and a $3\frac{1}{2}$-percent camber. The leading edge was sharpened to a 2° wedge angle by chamfering the upper surface as shown in figure 2 to allow the upper surface to ventilate at as low an angle as possible. The triangular hydrofoils had a continuously increasing radius of curvature from tip to root, whereas the radius of the rectangular hydrofoil was constant along the span. The basic projected aspect ratio of each hydrofoil was approximately 1.8. The hydrofoils had a two-dimensional design lift coefficient $C_{L,d}$ of 0.247 (ref. 2). The swept triangular hydrofoil had 21.7° sweep of the 50-percent-chord line.

APPARATUS AND PROCEDURE

A detailed description of Langley tank no. 1, the apparatus for towing the model, and the instrumentation for measuring the lift, drag, and pitching moment is given in reference 3. A photograph of model S on the towing gear is presented in figure 3.

The hydrofoils were attached to short struts, which in turn were attached to a mounting plate, as shown in figures 1 and 3. The angle of attack of the hydrofoils, which was measured in a vertical plane, was changed by rotating the mounting plate about a lateral axis through

the pivot (fig. 3). A deflector plate, seen in figures 3 and 4, kept the spray from being thrown up into the towing gear. The data obtained when the flow struck the deflector or the bottom of the mounting plate have been deleted, and therefore the data given represent forces on the hydrofoils alone.

The tests were made at constant speeds with the model free to rise. Generally two or three load conditions were obtained during each run by increasing the applied load. A few check runs were also made in which the applied load was decreased, and a few in which the load was held constant and the speed was increased. No significant differences were found in the results obtained by the various methods.

The wetted areas were determined from underwater photographs, or from visual wetted-length readings where photographs were not available. Typical underwater photographs of the three hydrofoils are shown in figure 4. The method and setup used for obtaining these photographs are described in reference 4. These wetted areas were considered to be the areas wetted on the undersurface and excluded spray wetting, which does not contribute appreciably to the lift force.

The visual depth readings were referred to the undisturbed water level. Corrections to these readings were necessary, however, because of a surge or long wave which is inherent in the tank during operation. These corrections were obtained by the method described in reference 5, where a vertically oscillating probe was used to measure the actual position of the water surface in the vicinity of the model. In this report the depth of submersion d is divided by the mean geometric chord c (0.3 foot for each of the three models) to nondimensionalize it.

The windage tares were obtained for the towing gear at various speeds, angles of attack, and vertical positions corresponding to a range of depths and applied as corrections to the load and resistance. The tares for pitching moment were found to be negligible.

The data were obtained at a number of constant speeds for various loads at each angle of attack. Motion pictures were taken of accelerated runs to observe the process of ventilation.

The quantities measured are believed to be accurate or reproducible within the following limitations:

Angle of attack (incidence), deg	±0.1
Depth of submersion, in.	±0.1
Load, lb	±0.2
Pitching moment, ft-lb	±1.0
Resistance, lb	±0.2

Speed, fps	±0.2
Wetted length (at leading or trailing edge), in.	±0.15

RESULTS AND DISCUSSION

Flow Characteristics

The changes in flow leading up to complete ventilation of the upper surface of the hydrofoils were determined from visual observations and the study of motion pictures taken during accelerated runs. In the case of the swept triangular hydrofoil, air entered along the blunt trailing edge as the speed was increased and flowed down to the tip. At sufficiently high angles of attack, a cavity formed at the leading edge near the tip and expanded toward the surface until the cavity enclosed the entire upper surface of the hydrofoil, which was completely ventilated to the atmosphere. Ventilation of the unswept triangular hydrofoil occurred in a similar manner except that, once air reached the tip, the cavity seemed to develop more rapidly.

A possible explanation for this difference in rapidity of cavity formation may be obtained by reviewing the mechanism of ventilation. As pointed out in reference 2, ventilation occurs when air is introduced into a region of the flow where the boundary layer is already separated. For example, air first comes down the trailing edge of the hydrofoils because of the separated flow in the wake of the blunt trailing edge. At some angle of attack boundary-layer separation also occurs along the leading edge of the hydrofoils. Because of the spanwise flow on the hydrofoils caused by the sweep, the chordwise extent of the leading-edge separated region is longest at the tip of model S and decreases toward the surface. On the other hand, the leading-edge separated region on model U is longer at the surface than at the tip. In both cases, the air at the tips contacts the separated region of the model and the lower region is immediately ventilated. The air then progressively ventilates the separated regions above it. This progressive ventilation up the foil will be more rapid if it moves into a region of increasing boundary-layer separation such as is found on model U rather than the region of decreasing separation found on model S.

Air entered along the blunt trailing edge of the rectangular hydrofoil and seemed to ventilate the upper surface almost instantaneously.

Full ventilation occurred regularly at angles of attack of 11° and higher for the swept triangular hydrofoil, at angles of 10° and higher for the unswept triangular hydrofoil, and at angles of 12° and higher for the rectangular hydrofoil.

As has previously been mentioned, data also are presented for the low angles of attack at which the upper surface is nonventilated or only partially ventilated. The nonventilated and partially ventilated flow conditions may be seen in figure 5 along with the fully ventilated flow condition for each hydrofoil.

A ventilated flow condition different from that of figure 5 is shown in figure 6. Here the flow adheres to the upper surface of the hydrofoil near the leading edge and separates at the upper-surface break, with ventilation occurring aft of this point. This condition was encountered only with the triangular hydrofoils and occurred at angles of attack of 8° or less. The discontinuity in the upper surface of the hydrofoil at the intersection between the flat and curved portions produces an abrupt adverse pressure gradient. This intersection is therefore a likely location for boundary-layer separation when the hydrofoil is at angles at which the forward flat section is wetted. The length of the separated region in this location is probably very short and may receive air from the blunt trailing edge on the triangular models. If the speed of the rectangular hydrofoil were increased sufficiently, a vapor cavity would form downstream of the upper-surface break and would extend to the trailing edge and become ventilated.

An attempt was made to induce separation at angles below those at which complete ventilation normally occurred. This was done by disturbing the flow immediately ahead of and at the leading edge of the hydrofoil with a sharp probe to allow air to enter at the upper surface of the hydrofoil. This caused a slight separation to occur; however, when the probe was removed, the cavity could not be sustained and it immediately closed.

Force Data

Originally the measured data were plotted directly in the form of lift, drag, and moment coefficients and were found to have some scatter. This scatter was generally attributable to the fact that the percentage error in the measured total wetted area increased with decrease in depth and became significantly great at the shallower depths. The data were then plotted as d/c, S, D/q, and M/qc against L/q, as shown in figures 7 to 10, respectively. The resulting points fall essentially on a single curve for each angle of attack. A cross plot from the faired curves of figures 7 to 10 therefore gave more accurate values of the coefficients, which are plotted in the later figures.

In general, the hydrofoils were fully ventilated at the high angles of attack. At angles below approximately 10°, most of the data were for either nonventilated or only partially ventilated conditions. The few

points at which complete ventilation did occur were generally obtained at high speeds and shallow depths (small values of L/q).

The pitching moment, which is presented in figure 10, was referred to a transverse axis passing through the tips of the triangular hydrofoils, or through the tips at the trailing edge for the rectangular hydrofoils. Negative pitching moments were obtained for the unswept triangular hydrofoil, in contrast to the positive pitching moments for the other hydrofoils, because of the choice of the moment reference. When the moments are taken about the tips, the moment reference for the unswept triangular hydrofoil is, in effect, at the leading edge as a result of the hydrofoil geometry.

Values of lift, drag, and pitching-moment coefficients were computed from the faired curves in figures 8, 9, and 10, respectively. Corresponding depth-chord ratios were obtained from figure 7. Symbols shown on the rest of the plots represent faired or computed data.

Lift coefficient.- The variations of lift coefficient with depth-chord ratio are presented in figure 11 for the three hydrofoils at all angles of attack of the investigation. The solid curves indicate the angles at which the hydrofoils were completely ventilated and the dashed curves indicate the angles at which only partial or no ventilation occurred. Because of their geometry, the triangular hydrofoils have approximately a constant wetted aspect ratio for each angle of attack regardless of depth, and only a small variation in the aspect ratio occurs throughout the angle-of-attack range. For these constant-aspect-ratio hydrofoils, the lift coefficient in the ventilated region would be substantially independent of depth if the cavitation number σ based on the ambient pressure corresponding to the mean hydrostatic pressure on the hydrofoil were zero. The data for the triangular hydrofoils, however, show a gradual increase in lift coefficient with increase in depth of submersion at the angles at which the hydrofoils are fully ventilated. Some of the increase in lift coefficient is due to the increase in cavitation number caused by the hydrostatic head on the hydrofoil. The large increase in lift coefficient with depth of submersion for the rectangular hydrofoil would be expected because of the increase in wetted aspect ratio b^2/S from 0.4 to about 0.9 with increase in depth-chord ratio from 0.4 to 0.8.

The lift coefficients for the three hydrofoils are compared in figure 12, where the variation in lift coefficient with angle of attack is shown for depth-chord ratios of 0.4 and 0.8. The break in each of the curves indicates the approximate angle at which complete ventilation of the hydrofoil occurred as the angle of attack was increased. No abrupt change in lift coefficient occurred with an increase in angle of attack from the low angles to the higher angles at which the hydrofoils become fully ventilated. At the angles where full ventilation occurs, the lift

coefficient increased linearly with increase in angle of attack for all three hydrofoils. For a given angle of attack and depth of submersion in the ventilated region, the swept triangular hydrofoil had a higher lift coefficient than the other hydrofoils. As might be expected, the rectangular hydrofoil had the lowest lift coefficients since it operates at a small wetted aspect ratio as compared with that of approximately 1.8 to 1.9 for the triangular hydrofoils.

Drag coefficient.- The variation of drag coefficient with depth-chord ratio is presented for each hydrofoil in figure 13. The drag coefficients for the three hydrofoils are compared in figures 14 and 15, where the variation in drag coefficient with angle of attack and with lift coefficient, respectively, is shown for depth-chord ratios of 0.4 and 0.8. The break in the curves again indicates the separation between complete ventilation and partial or no ventilation.

The drag-coefficient curves in figure 14, like the lift-coefficient curves in figure 12, show no abrupt change as the angle of attack is increased and the hydrofoils become fully ventilated. For a given angle of attack, the value of the drag coefficient is about the same for both triangular hydrofoils. The drag coefficient for the rectangular hydrofoil is much lower than that for the triangular hydrofoils at a depth-chord ratio of 0.4, and approaches the value for the triangular hydrofoils at a depth-chord ratio of 0.8.

For a given value of the lift coefficient (fig. 15), the swept triangular hydrofoil has less drag than the other hydrofoils, except that at the depth-chord ratio of 0.8 the rectangular hydrofoil has about the same drag as the swept-triangular hydrofoil.

Lift-drag ratio.- The variation in lift-drag ratio with depth-chord ratio is presented in figure 16 for the three hydrofoils at all angles of attack of the investigation. There is a gradual increase in lift-drag ratio with increase in submergence of the triangular hydrofoils at all angles of attack. The lift-drag ratio for the rectangular hydrofoil, however, shows a substantial increase with increase in depth of submersion, largely because of the increase in wetted aspect ratio at the deeper submersions.

The lift-drag ratios for the three hydrofoils are compared in figures 17 and 18, where the variation in lift-drag ratio with angle of attack and with lift coefficient, respectively, is shown for depth-chord ratios of 0.4 and 0.8. For a given angle of attack in the ventilated region, there is only a 10-percent maximum variation in the lift-drag ratio for the three hydrofoils (fig. 17). The lift-drag ratios in the ventilated region were about 4.0 at angles around 12° and decreased to about 2.5 at an angle of attack of 20°. The maximum

lift-drag ratios, however, occurred in the partially ventilated region at angles of attack between 6° and 8°, the swept-triangular hydrofoil having the maximum ratio of about 5.3 at a depth-chord ratio of 0.8.

For a given value of the lift coefficient in the ventilated region, it may be seen from figure 18 that the swept triangular hydrofoil had a higher lift-drag ratio than the other hydrofoils tested, particularly at the shallower depth-chord ratio of 0.4. In general, of the two triangular hydrofoils, which had equal aspect ratios regardless of depth, the swept triangular hydrofoil had better overall lift-drag ratios than the unswept triangular hydrofoil.

Pitching-moment coefficient.- The pitching-moment coefficients are plotted against depth-chord ratio in figure 19. The pitching moments for the unswept triangular hydrofoil are negative, as previously stated, because, in effect, the moment reference is at the leading edge on this hydrofoil.

Figure 20 shows a cross plot of figure 19 against angle of attack for depth-chord ratios of 0.4 and 0.8. A comparison of the swept triangular and the rectangular hydrofoils, which have the same relative moment reference, shows that the rectangular hydrofoil has greater positive moments at both depths in the ventilated region.

Comparison of experiment and theory.- Lift-drag ratios for three representative wetted aspect ratios of a planing flat plate (from refs. 6 and 7) are compared in figure 21 with the lift-drag ratios of the swept triangular hydrofoil at a depth-chord ratio of 0.8 and an aspect ratio of 1.8. At a given lift coefficient, the hydrofoil has a lower lift-drag ratio than the planing surface at the same aspect ratio. The lift-drag ratio of the planing surface at an aspect ratio of 0.5 is about the same as that of the hydrofoil. Since the maximum resistance of a hydro-ski-equipped craft usually occurs when the hydro-ski is fully wetted, the lift-drag ratio at an aspect ratio of 0.17 (length-beam ratio of 6), which represents this condition, also is shown. At the same lift coefficient, the hydrofoil is seen to have a higher lift-drag ratio than the planing surface with an aspect ratio of 0.17. The principal reason that the hydrofoil has lower lift-drag ratios than a planing flat plate of the same aspect ratio is the large dihedral of the hydrofoil. Also shown in figure 21 are data from reference 8 for a planing surface with 40° dead rise and an aspect ratio of 1.8. It may be seen that dead rise greatly reduces the lift-drag ratio, and the hydrofoil has a greater lift-drag ratio at a given lift coefficient than the planing surface with 40° dead rise.

In figure 22 the experimental lift-drag ratios for the swept triangular hydrofoil are compared with the theoretical lift-drag ratios

from reference 2 for a circular-arc hydrofoil at zero cavitation number. Theoretically the hydrodynamic coefficients depend on the local depth-chord ratio, which for this hydrofoil varies along the span. To simplify the calculation, an average value of 0.5 was assumed for the local depth-chord ratio. The theoretical forces were modified for 45° dihedral angle and 21.7° sweep of the 50-percent-chord line and comparisons were made for the same aspect ratio. The lift coefficients and lift-drag ratios for the hydrofoil were found to be in good agreement with those predicted by theory.

CONCLUDING REMARKS

The results of an investigation of the hydrodynamic forces on three surface-piercing supercavitating hydrofoils with 45° negative dihedral indicate that complete ventilation occurred at angles of attack of 11° and higher for the triangular hydrofoil with leading-edge sweep, at angles of 10° and higher for the triangular hydrofoil without leading-edge sweep, and at angles of 12° and higher for the rectangular hydrofoil. Of the two triangular hydrofoils, which had equal aspect ratios regardless of depth, the one with leading-edge sweep had somewhat better overall lift-drag ratios. The maximum lift-drag ratios obtained with the swept-leading-edge triangular hydrofoil were 5.3 in the low-angle partially ventilated region and 4.0 in the fully ventilated region at a depth-chord ratio of 0.8. No abrupt change in lift or drag occurred with an increase in angle of attack from the low angles to the higher angles at which the hydrofoils became fully ventilated. In the region of complete ventilation, the lift coefficient increased linearly with increase in angle of attack for all three hydrofoils. A brief comparison shows the experimental data to be in good agreement with that predicted by theory.

Langley Research Center,
National Aeronautics and Space Administration,
Langley Field, Va., February 10, 1960.

REFERENCES

1. Tulin, M. P., and Burkart, M. P.: Linearized Theory for Flows About Lifting Foils at Zero Cavitation Number. Rep. C-638, David W. Taylor Model Basin, Navy Dept., Feb. 1955.

2. Johnson, Virgil E., Jr.: Theoretical and Experimental Investigation of Arbitrary Aspect Ratio, Supercavitating Hydrofoils Operating Near the Free Water Surface. NACA RM L57I16, 1957.

3. Truscott, Starr: The Enlarged N.A.C.A. Tank, and Some of Its Work. NACA TM 918, 1939.

4. Kapryan, Walter J., and Weinstein, Irving: The Planing Characteristics of a Surface Having a Basic Angle of Dead Rise of 20° and Horizontal Chine Flare. NACA TN 2804, 1952.

5. Blanchard, Ulysse J.: The Planing Characteristics of a Surface Having a Basic Angle of Dead Rise of 40° and Horizontal Chine Flare. NACA TN 2842, 1952.

6. Weinstein, Irving, and Kapryan, Walter J.: The High-Speed Planing Characteristics of a Rectangular Flat Plate Over a Wide Range of Trim and Wetted Length. NACA TN 2981, 1953.

7. Shuford, Charles L., Jr.: A Theoretical and Experimental Study of Planing Surfaces Including Effects of Cross Section and Plan Form. NACA Rep. 1355, 1958. (Supersedes NACA TN 3939.)

8. Chambliss, Derrill B., and Boyd, George M., Jr.: The Planing Characteristics of Two V-Shaped Prismatic Surfaces Having Angles of Dead Rise of 20° and 40°. NACA TN 2876, 1953.

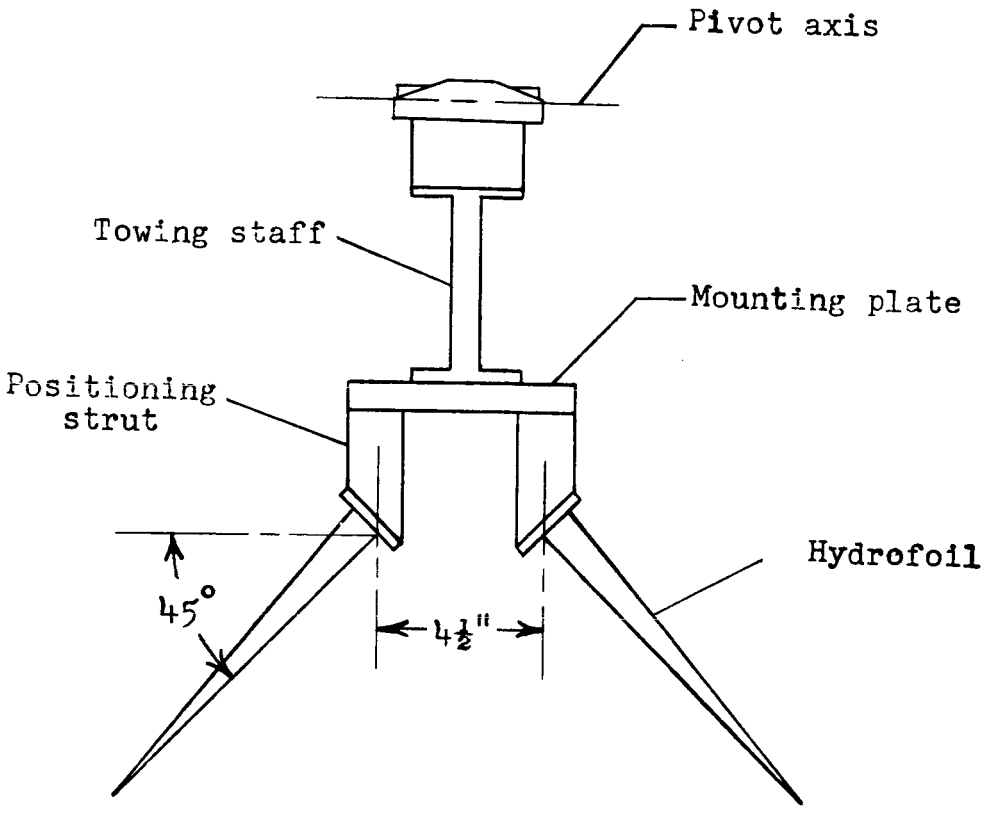

Figure 1.- General arrangement of hydrofoil system.

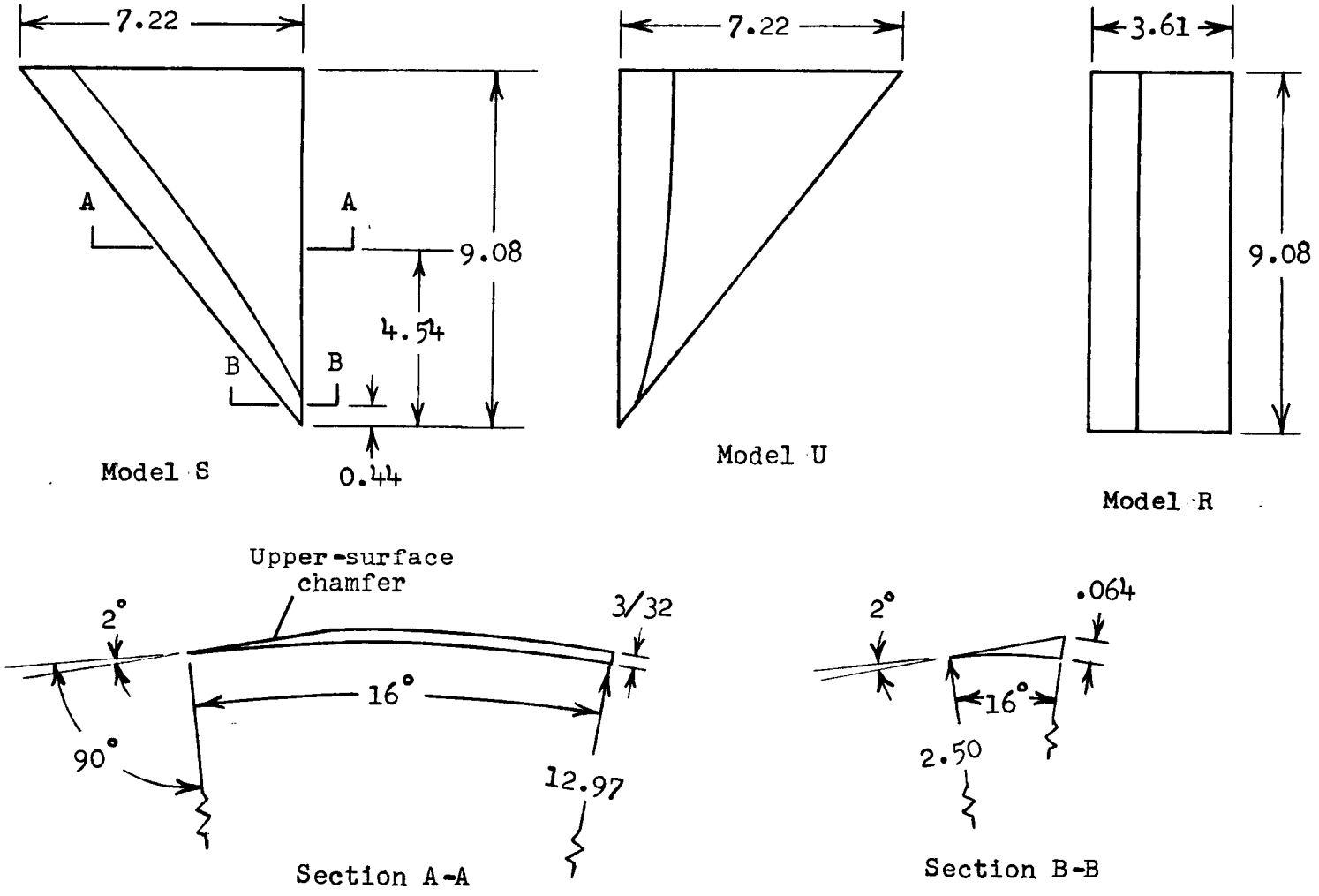

(Sections not shown to same scale)

Figure 2.- Plan form and sections of models. (Dimensions are in inches.)

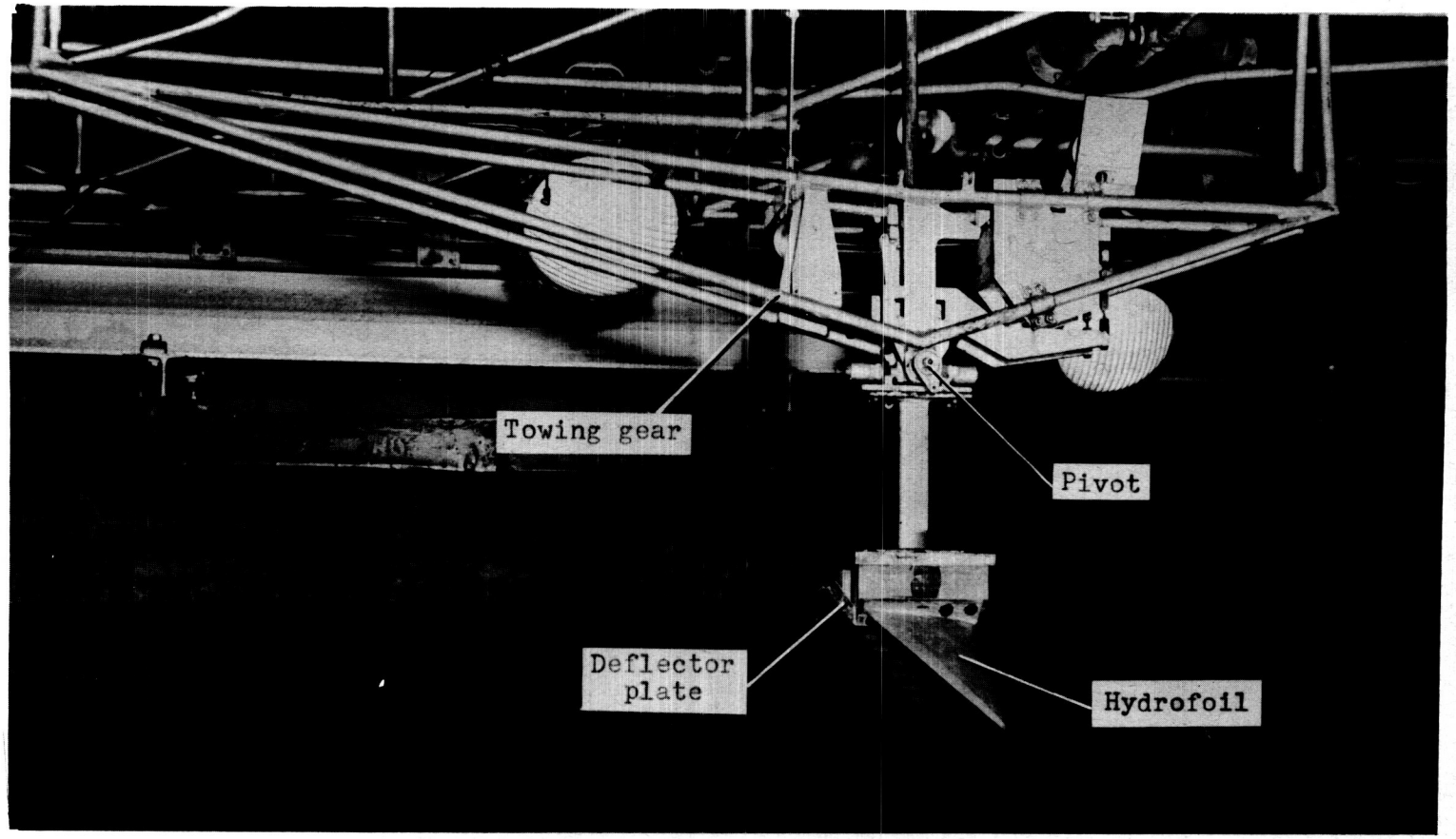

Figure 3.- Hydrofoil model S on towing gear. L-60-232

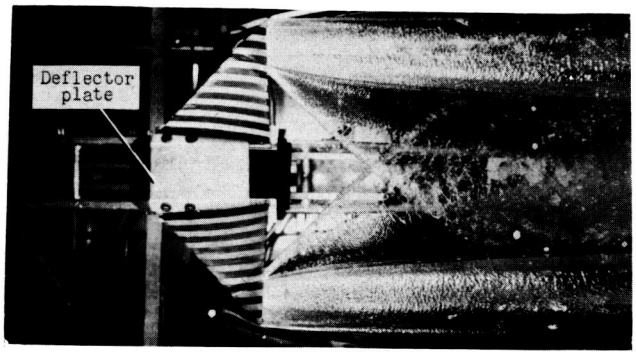

(a) Model S.

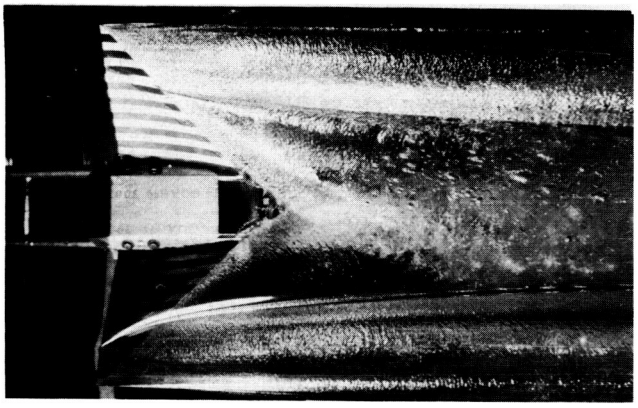

(b) Model U.

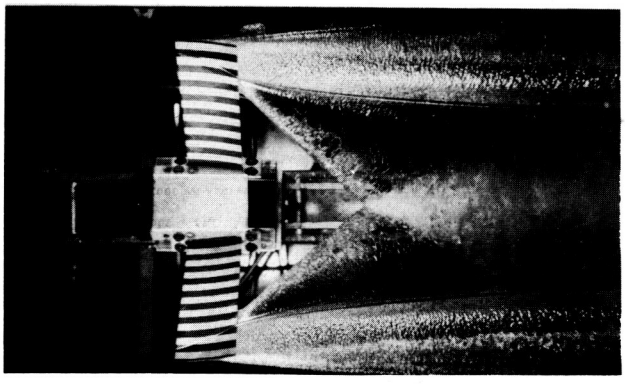

(c) Model R.

L-60-228

Figure 4.- Typical underwater photographs. $\alpha = 12^{\circ}$; L = 10 lb; V = 40 fps.

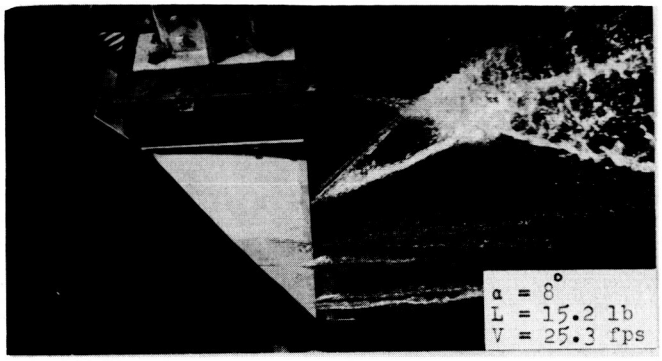

Nonventilated

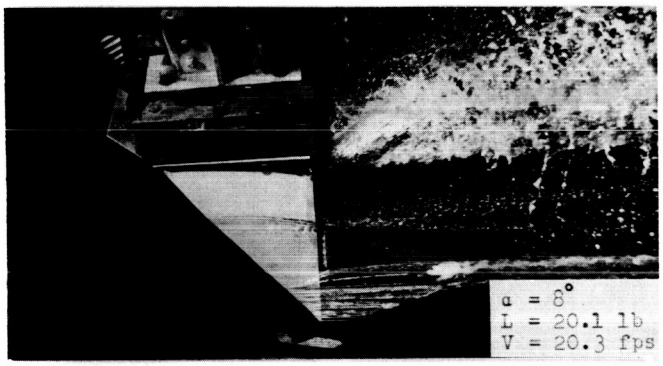

Partially ventilated

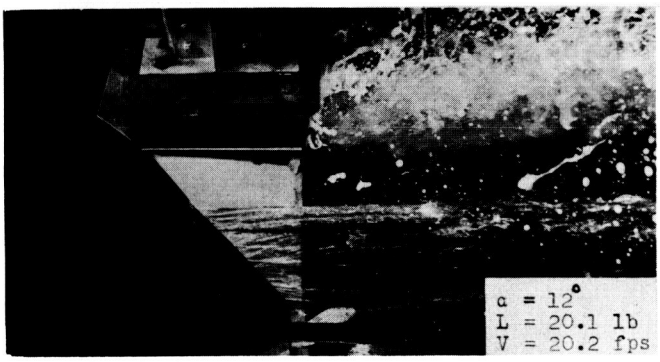

Fully ventilated

(a) Model S. L-60-229

Figure 5.- Photographs showing various flow conditions for all three hydrofoils.

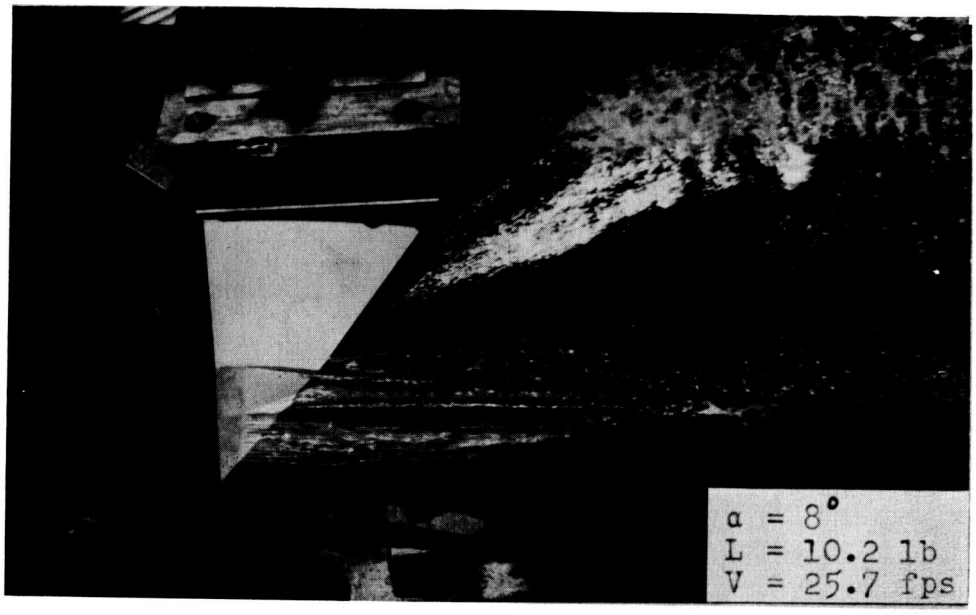

Partially ventilated

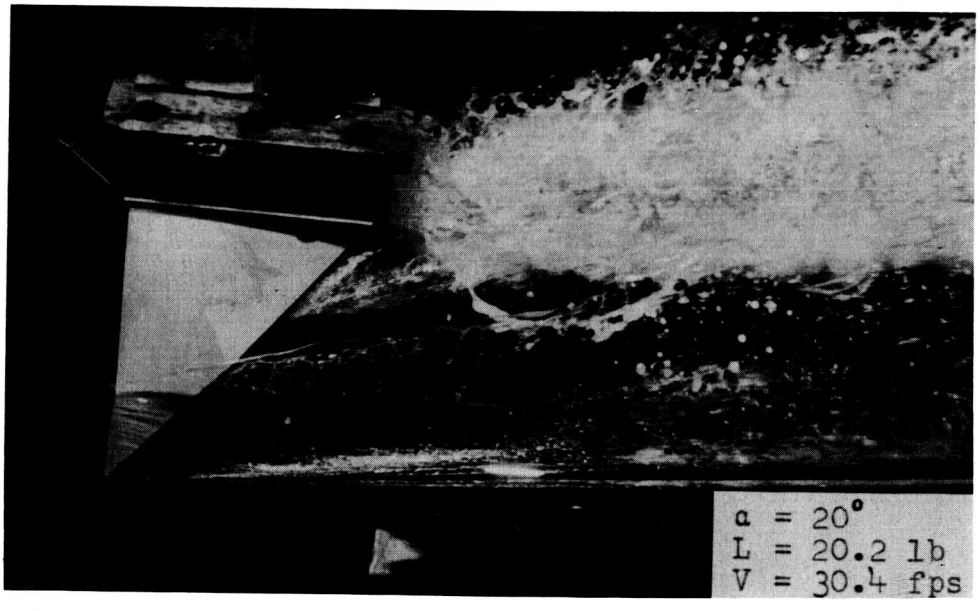

Fully ventilated

(b) Model U. L-60-230

Figure 5.- Continued.

Partially ventilated

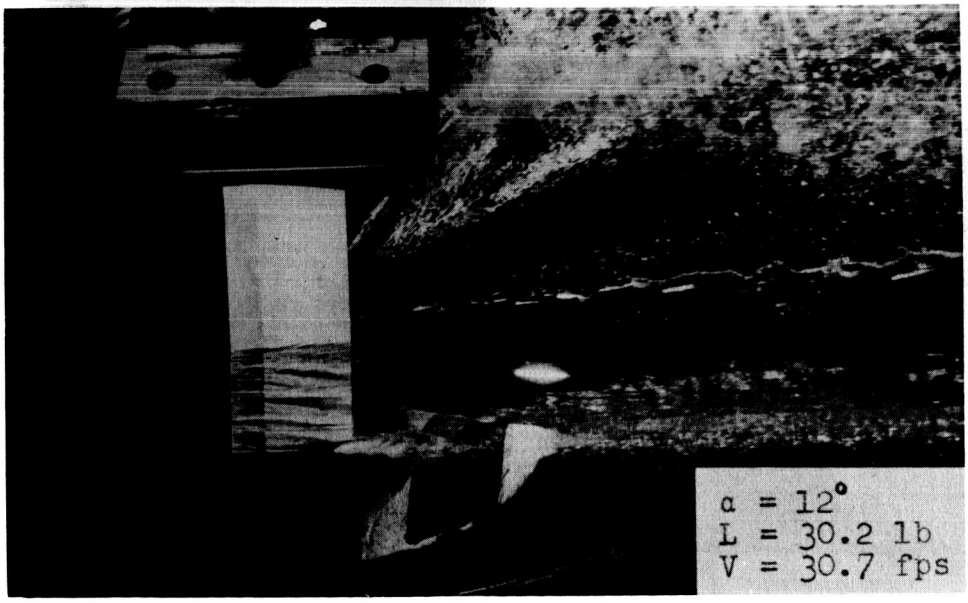

Fully ventilated

(c) Model R. L-60-231

Figure 5.- Concluded.

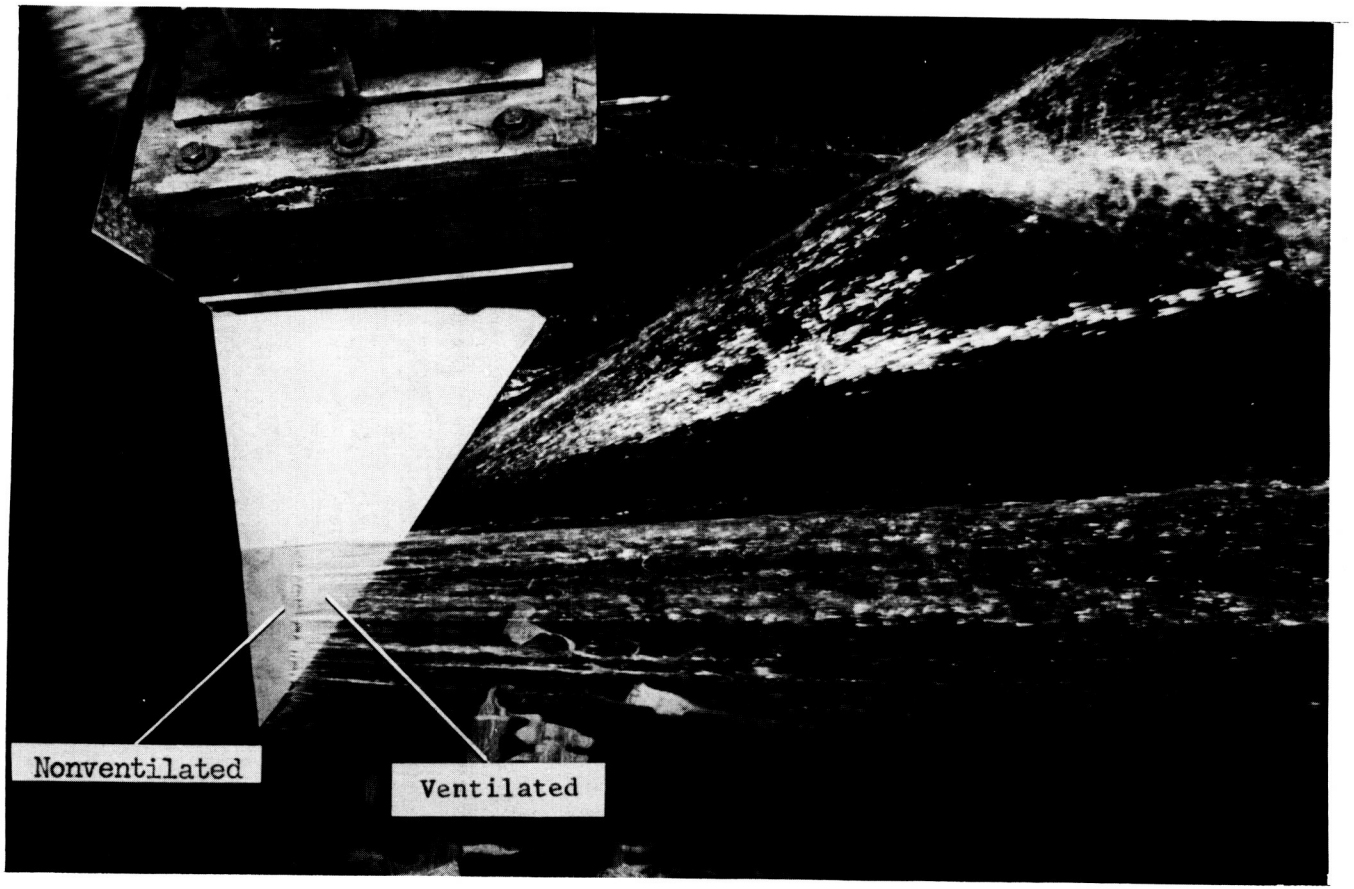

L-60-233

Figure 6.- Photograph of model U showing flow condition in which ventilation occurs aft of the upper-surface break. $\alpha = 4^{\circ}$; L = 5 lb; V = 40 fps.

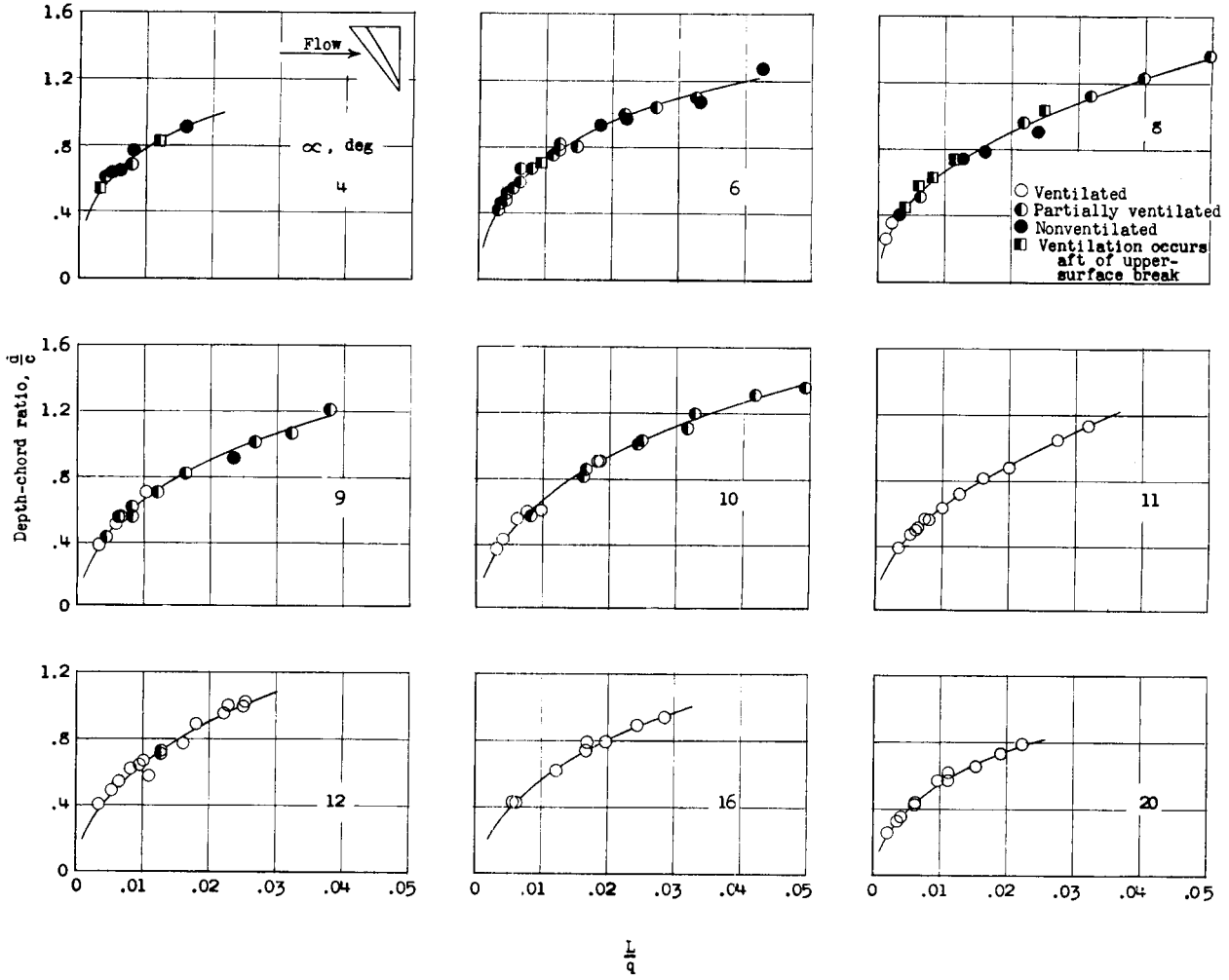

(a) Model S.

Figure 7.- Variation of depth-chord ratio with L/q.

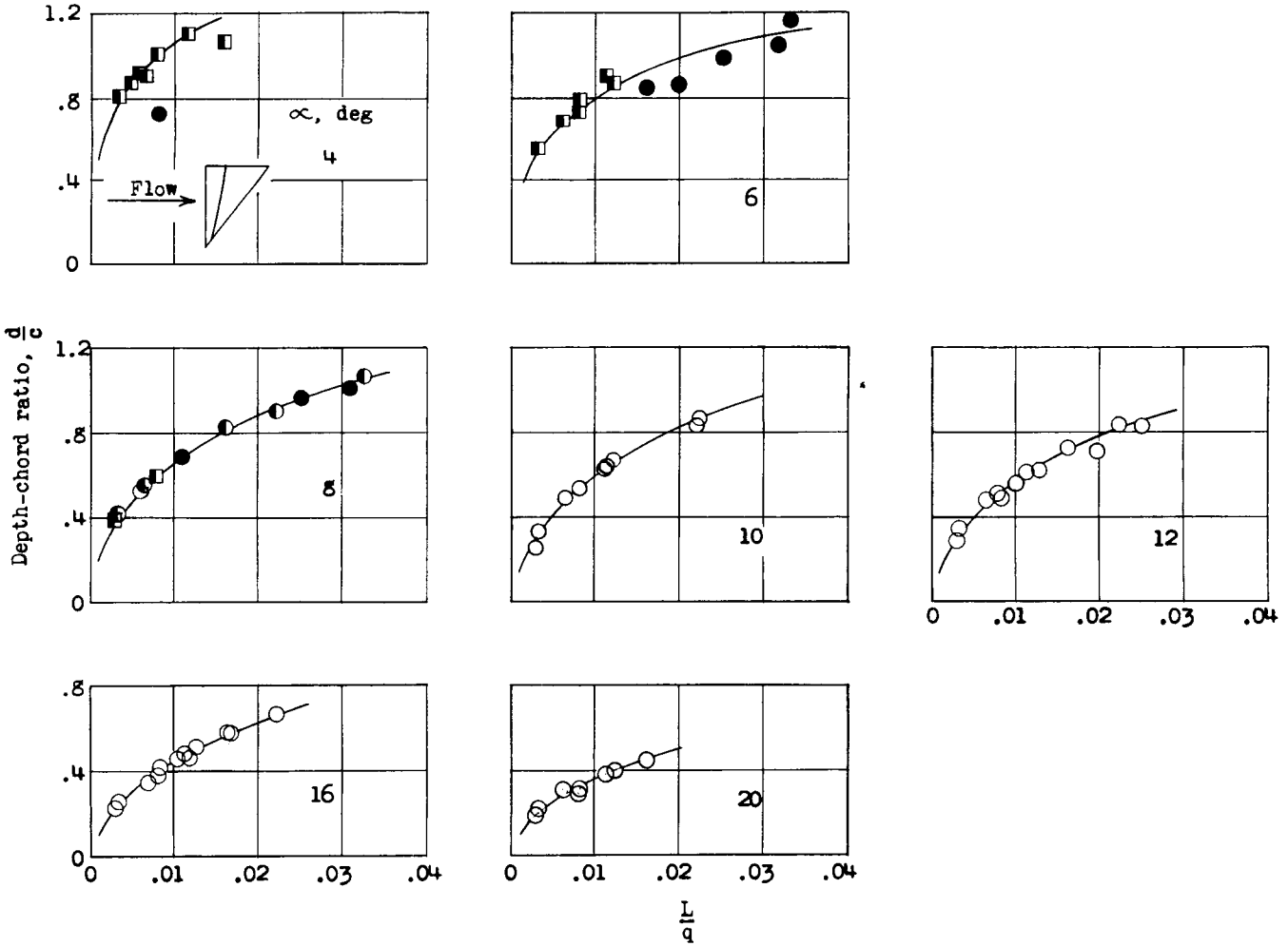

(b) Model U.

Figure 7.- Continued.

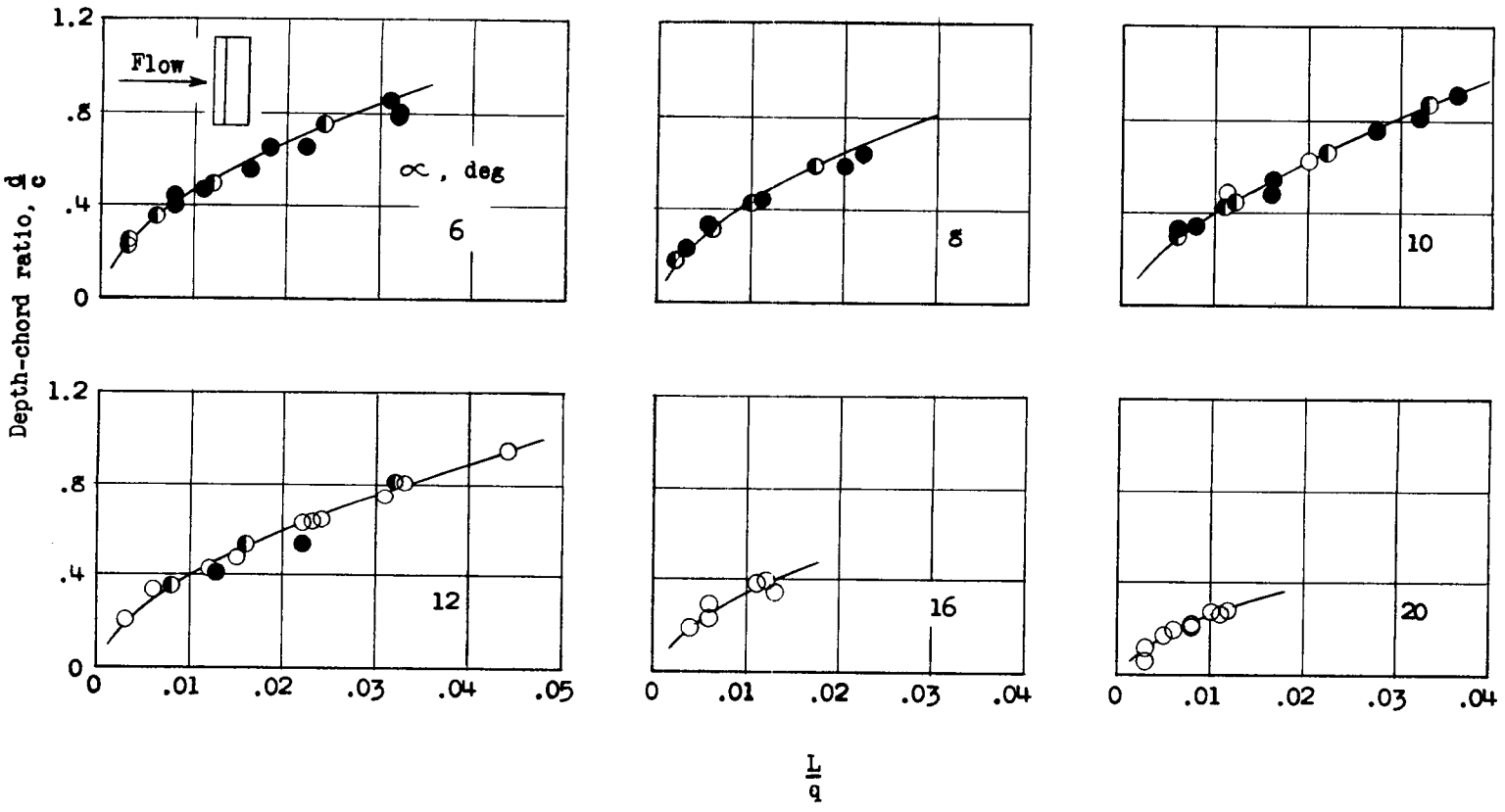

(c) Model R.

Figure 7.- Concluded.

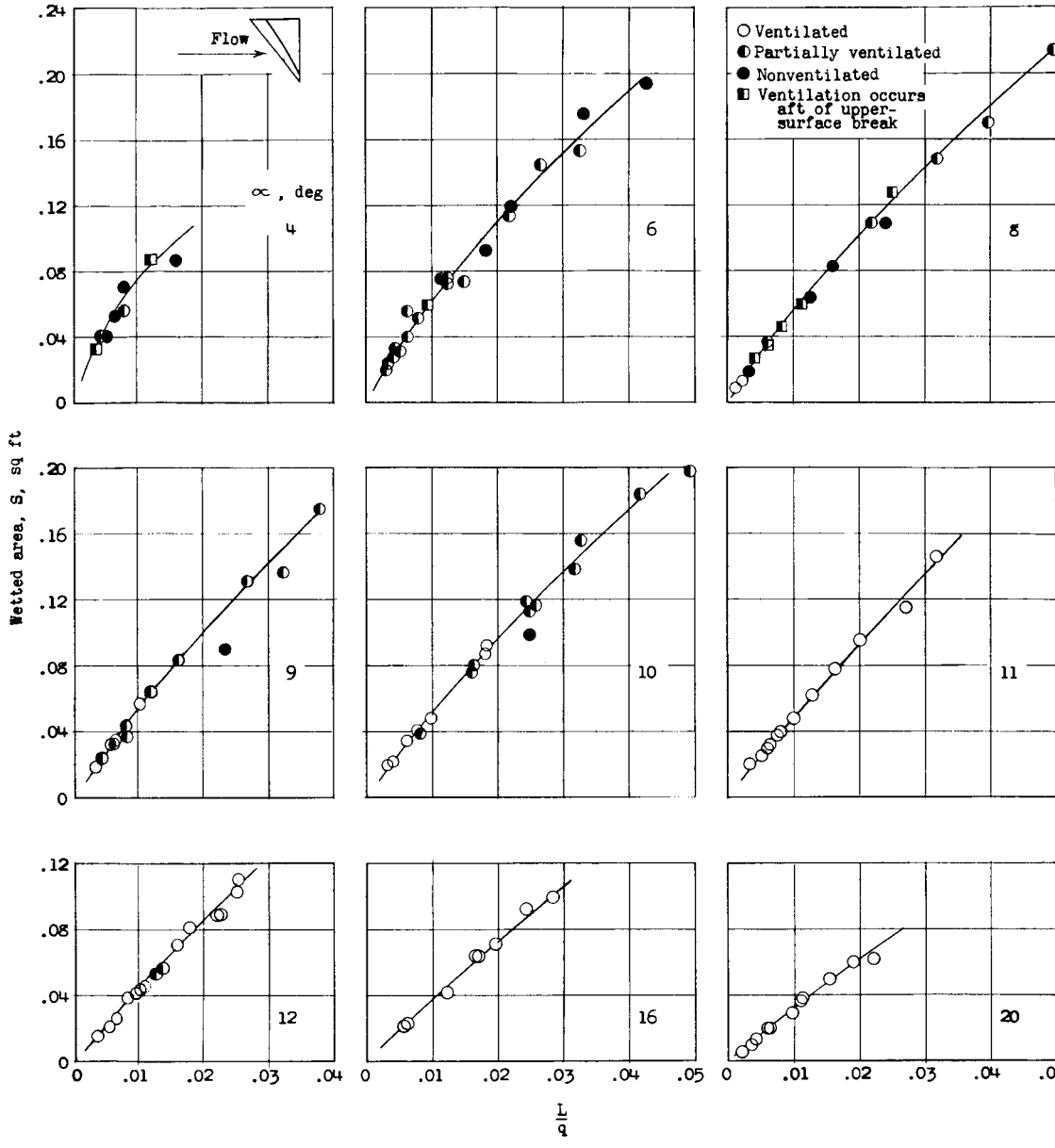

(a) Model S.

Figure 8.- Variation of wetted area with L/q.

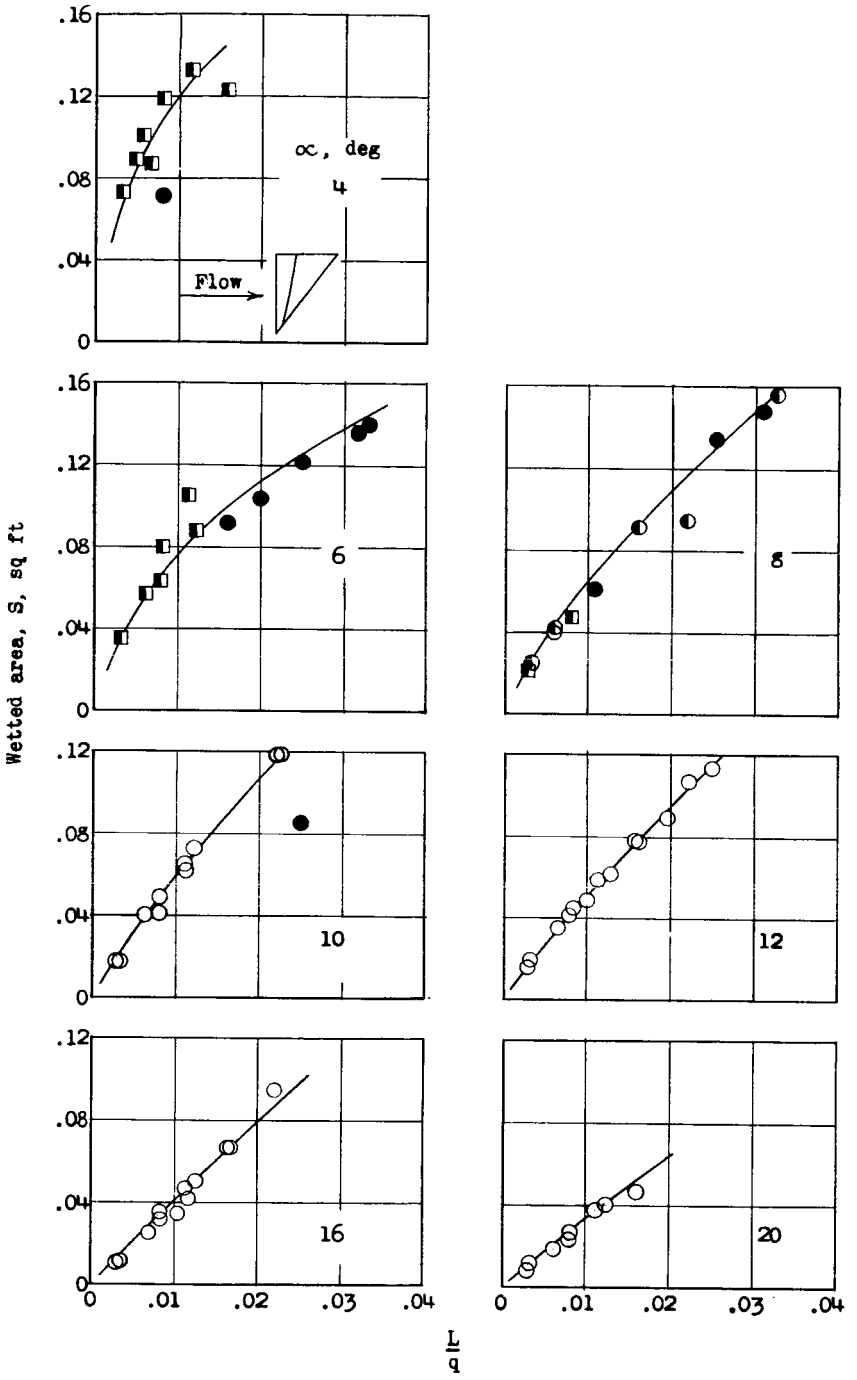

(b) Model U.

Figure 8.- Continued.

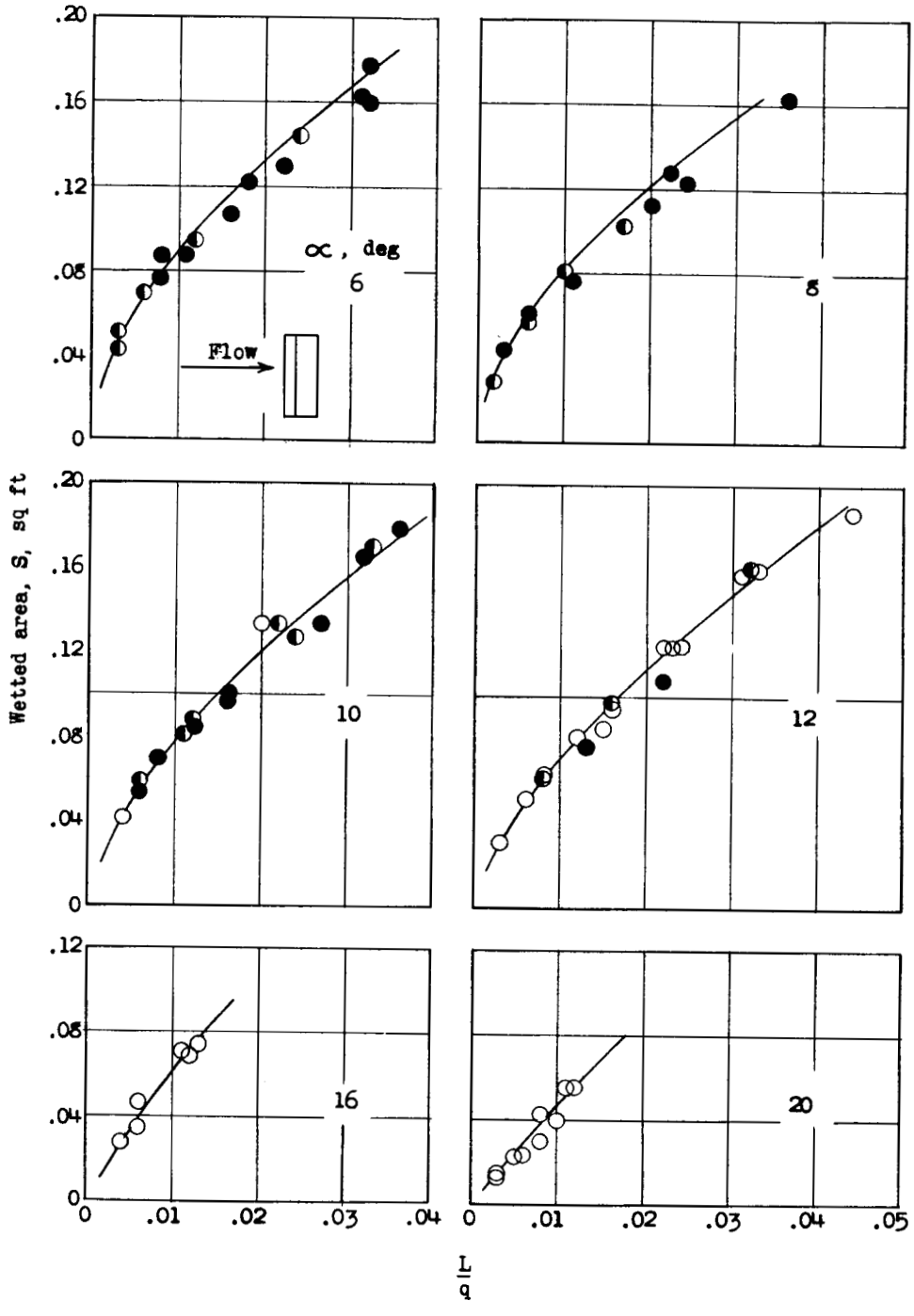

(c) Model R.

Figure 8.- Concluded.

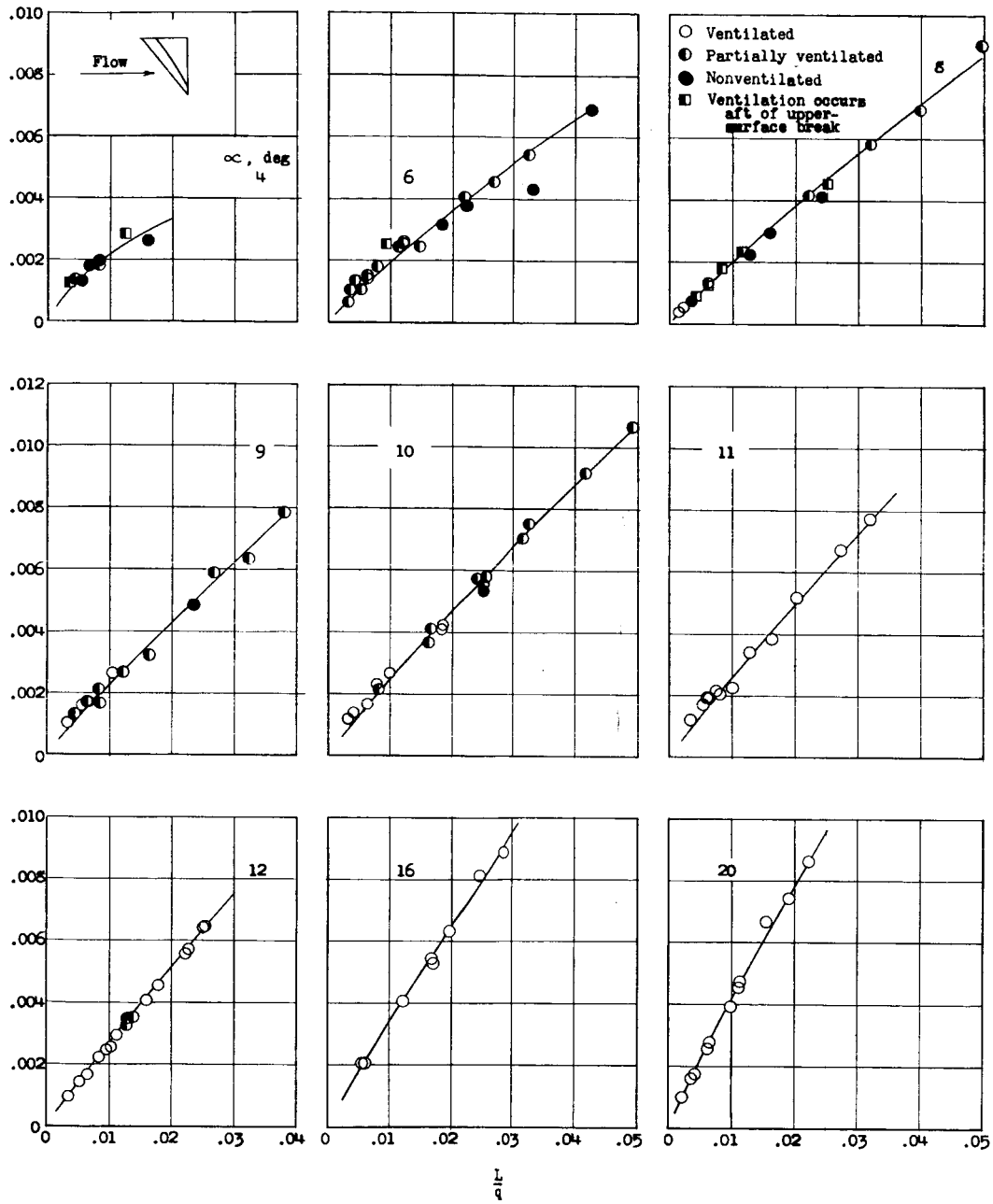

(a) Model S.

Figure 9.- Variation of D/q with L/q.

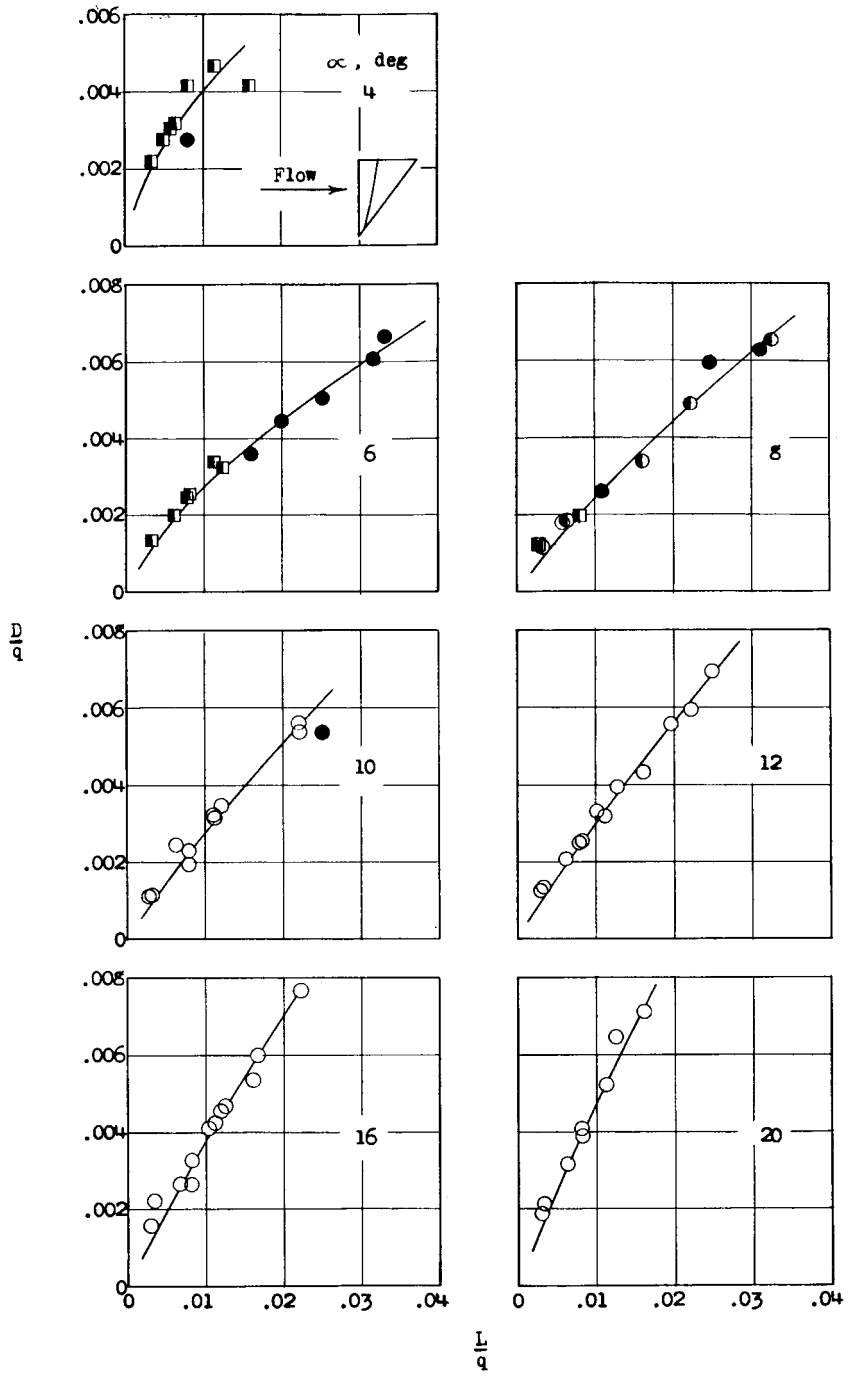

(b) Model U.

Figure 9.- Continued.

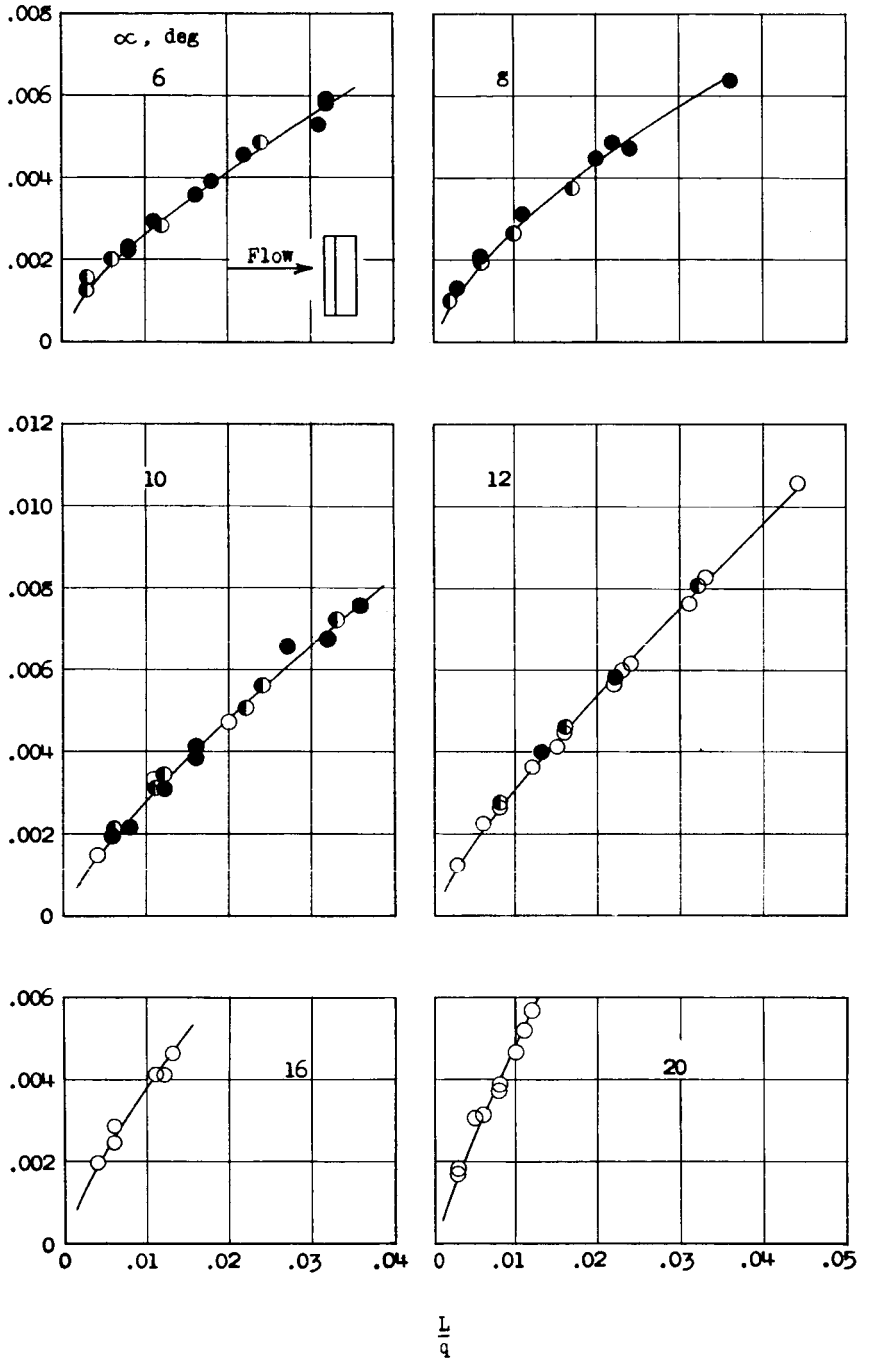

(c) Model R.

Figure 9.- Concluded.

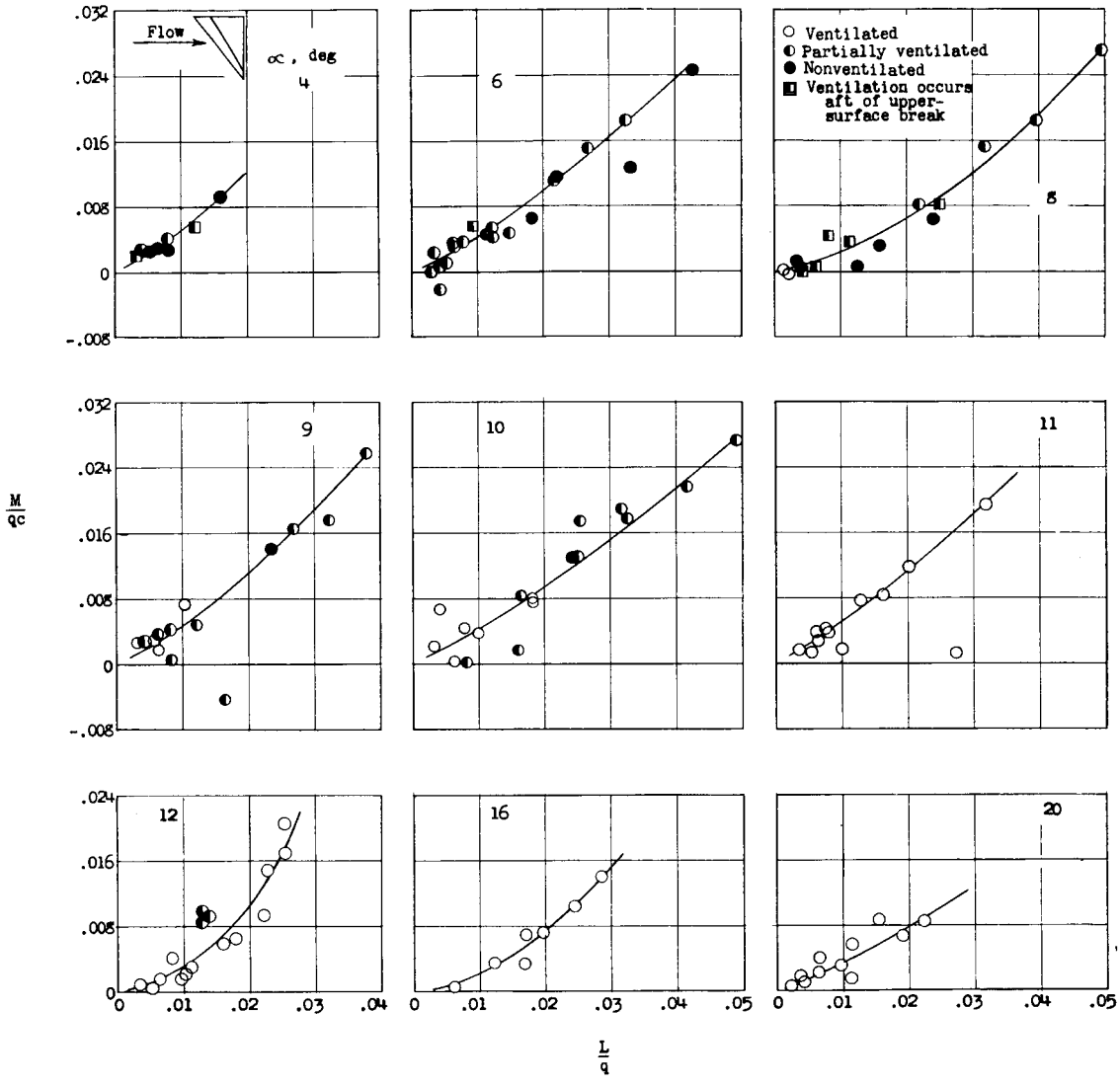

(a) Model S.

Figure 10.- Variation of M/qc with L/q.

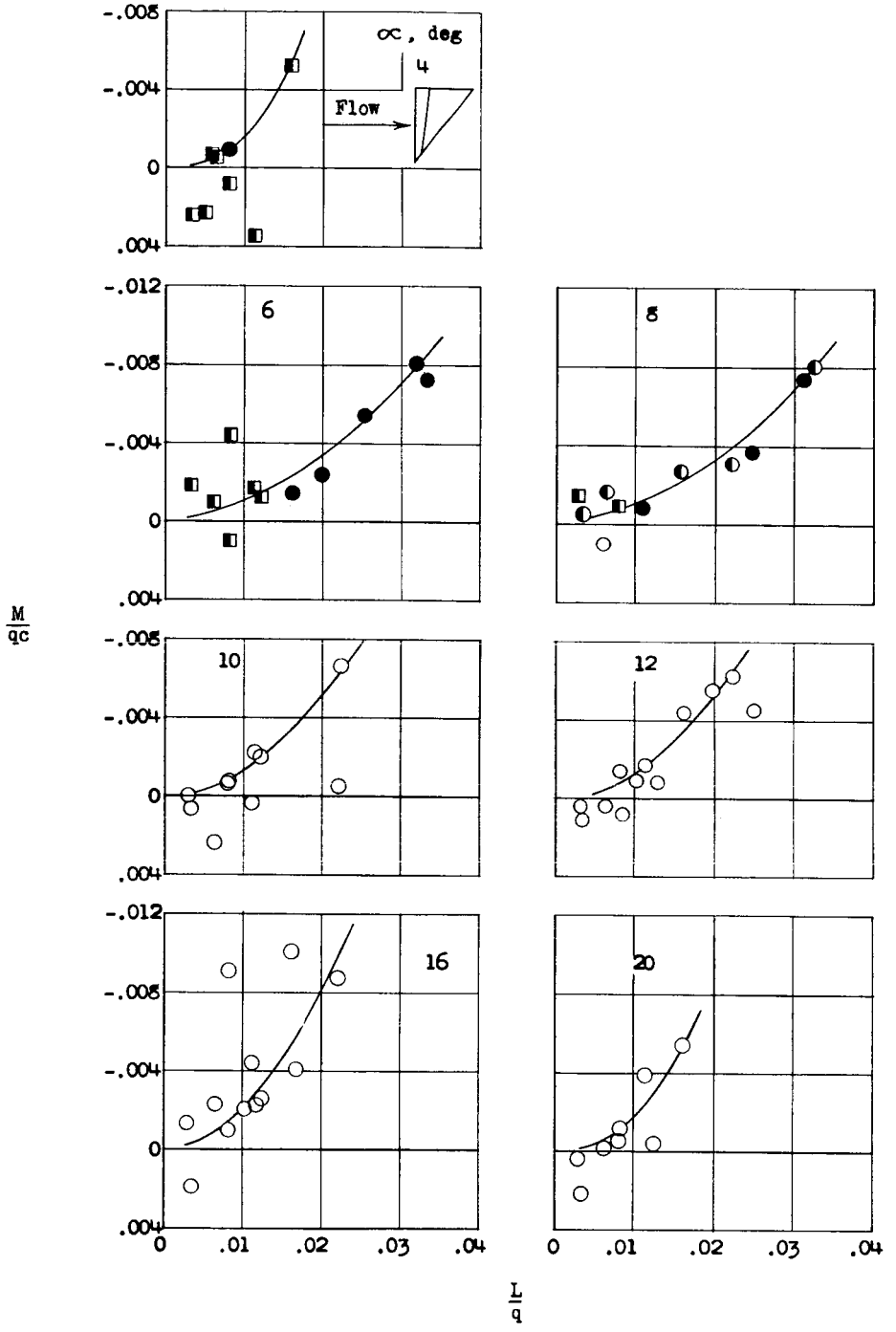

(b) Model U.

Figure 10.- Continued.

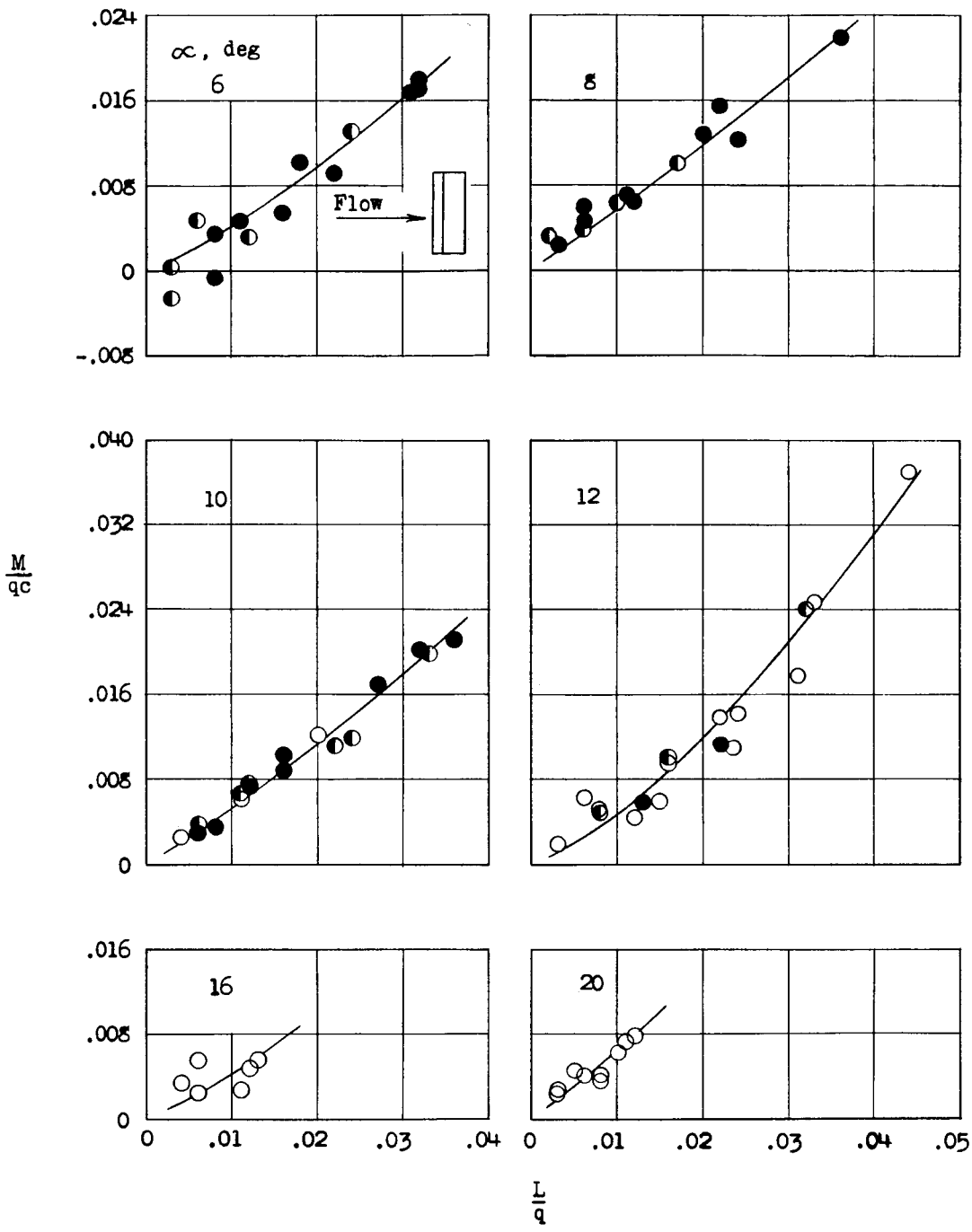

(c) Model R.

Figure 10.- Concluded.

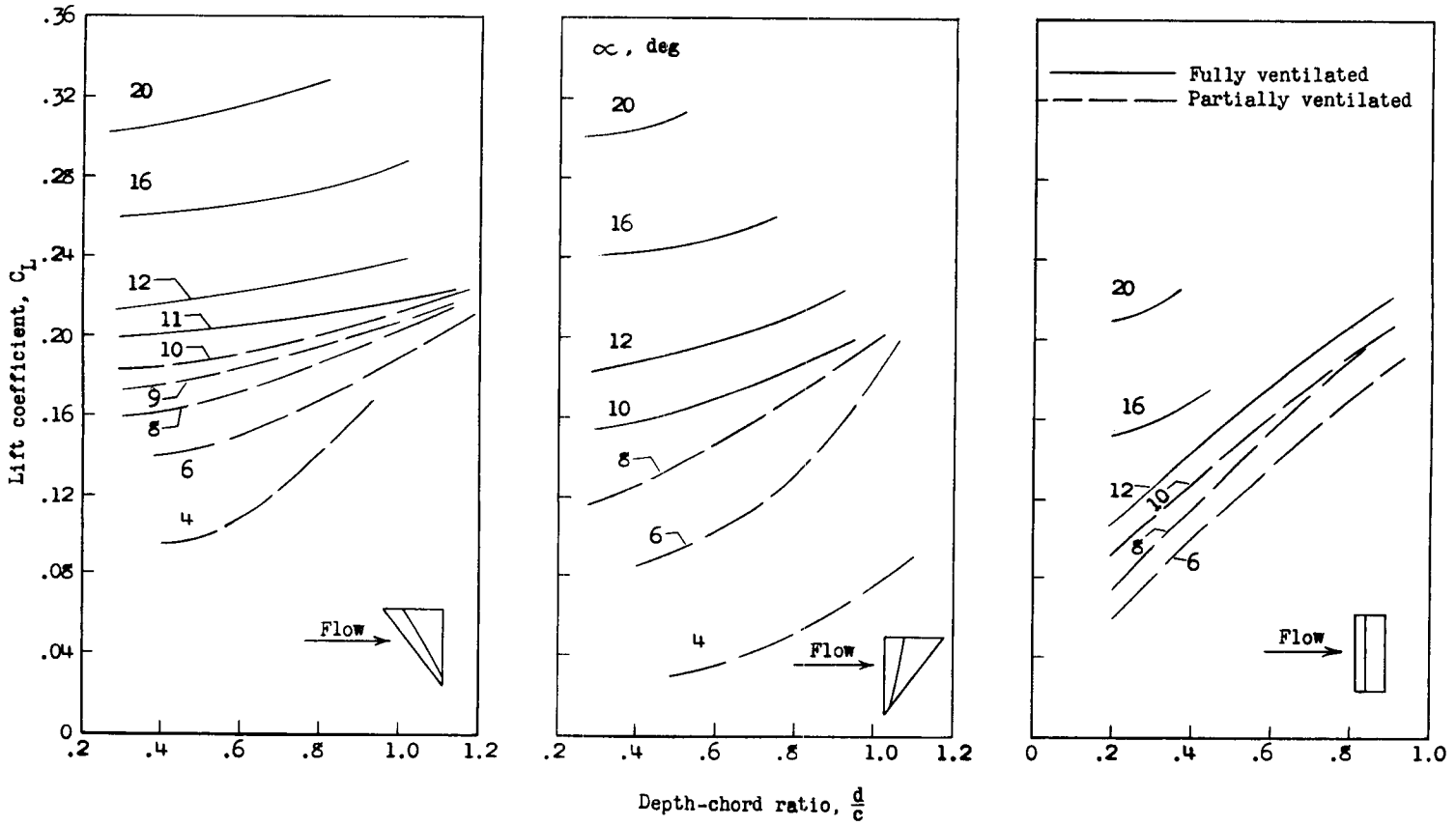

(a) Model S. (b) Model U. (c) Model R.

Figure 11.- Effect of depth of submersion on the lift coefficient.

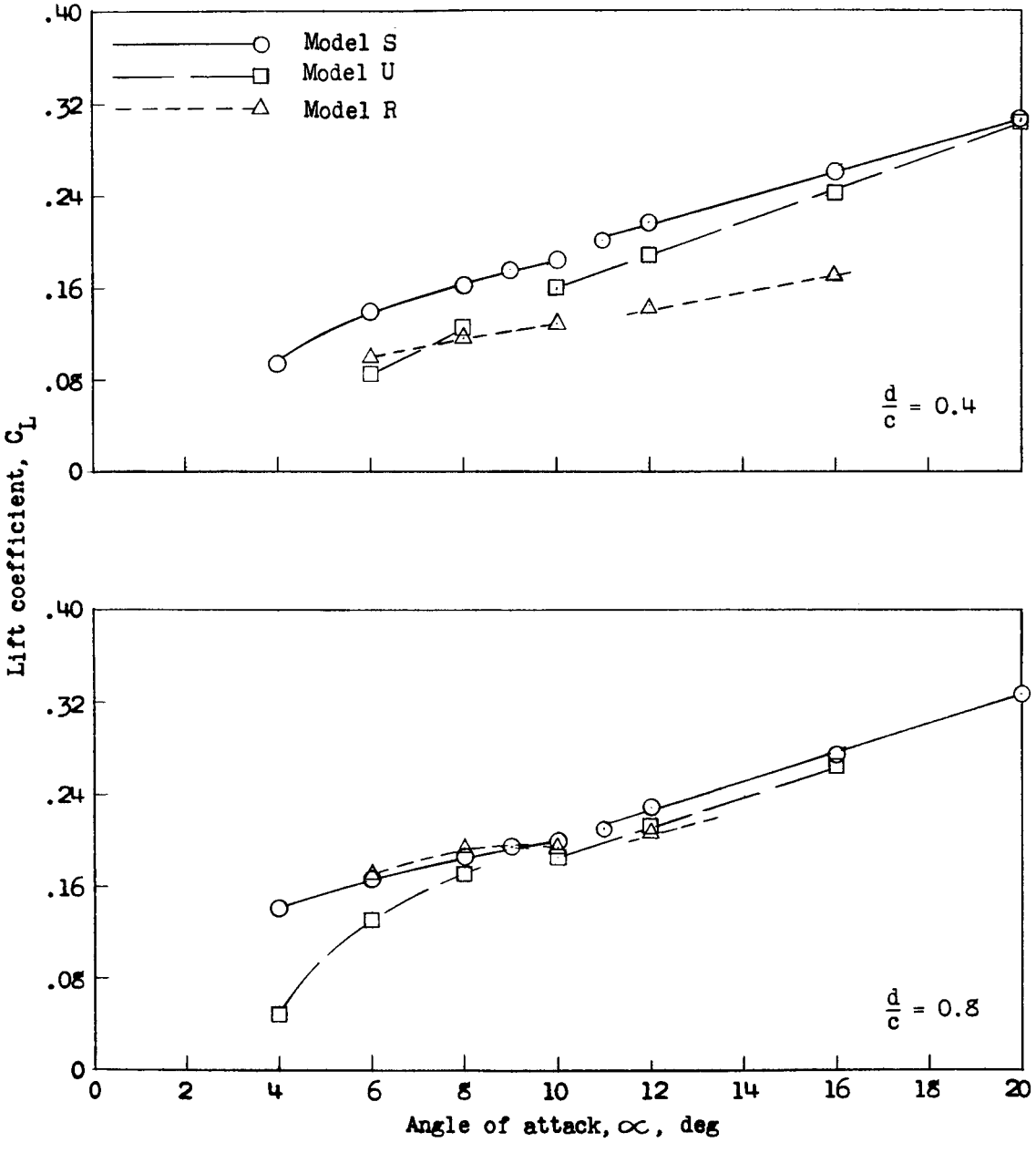

Figure 12.- Variation of lift coefficient with angle of attack.

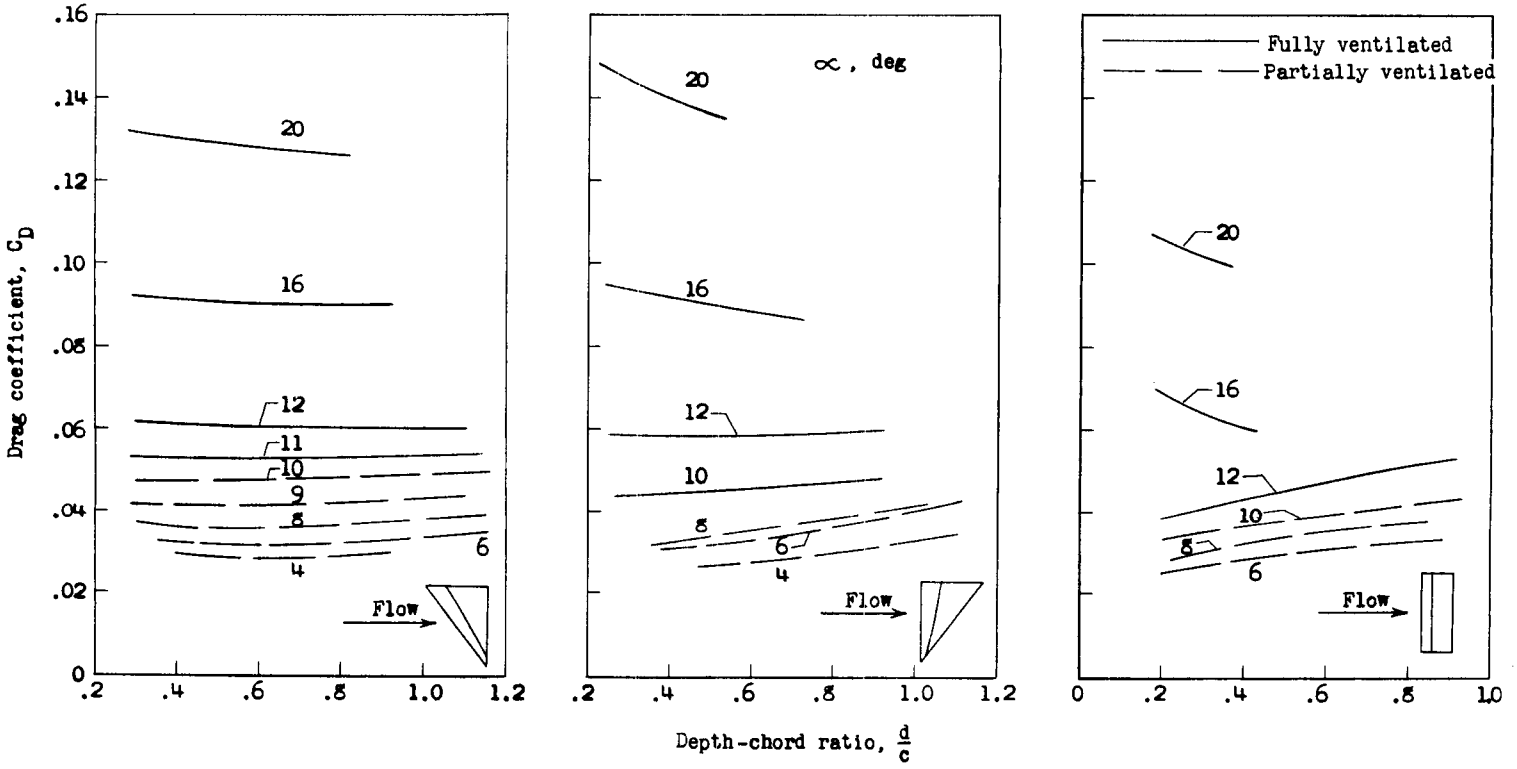

(a) Model S. (b) Model U. (c) Model R.

Figure 13.- Effect of depth of submersion on the drag coefficient.

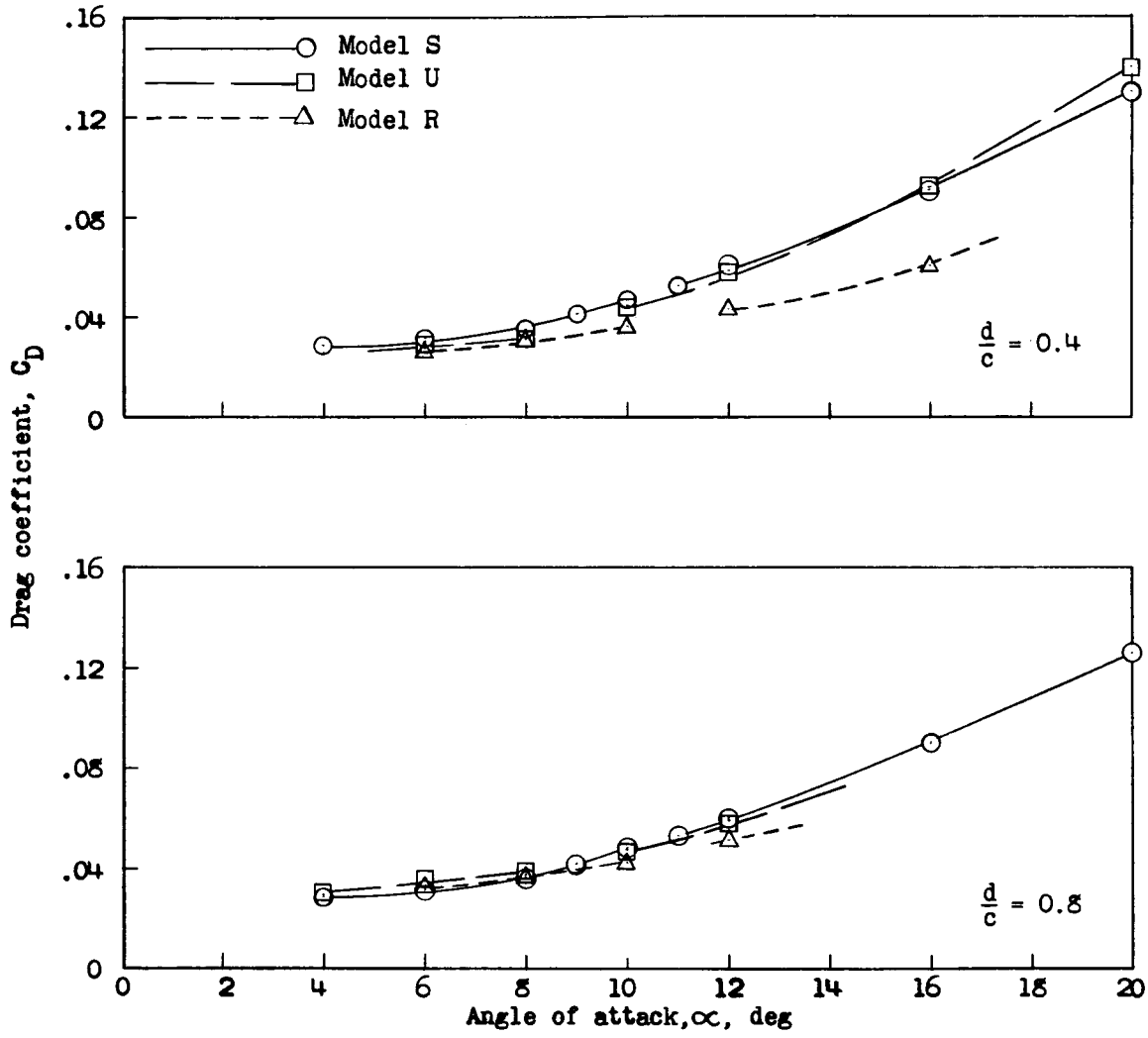

Figure 14.- Variation of drag coefficient with angle of attack.

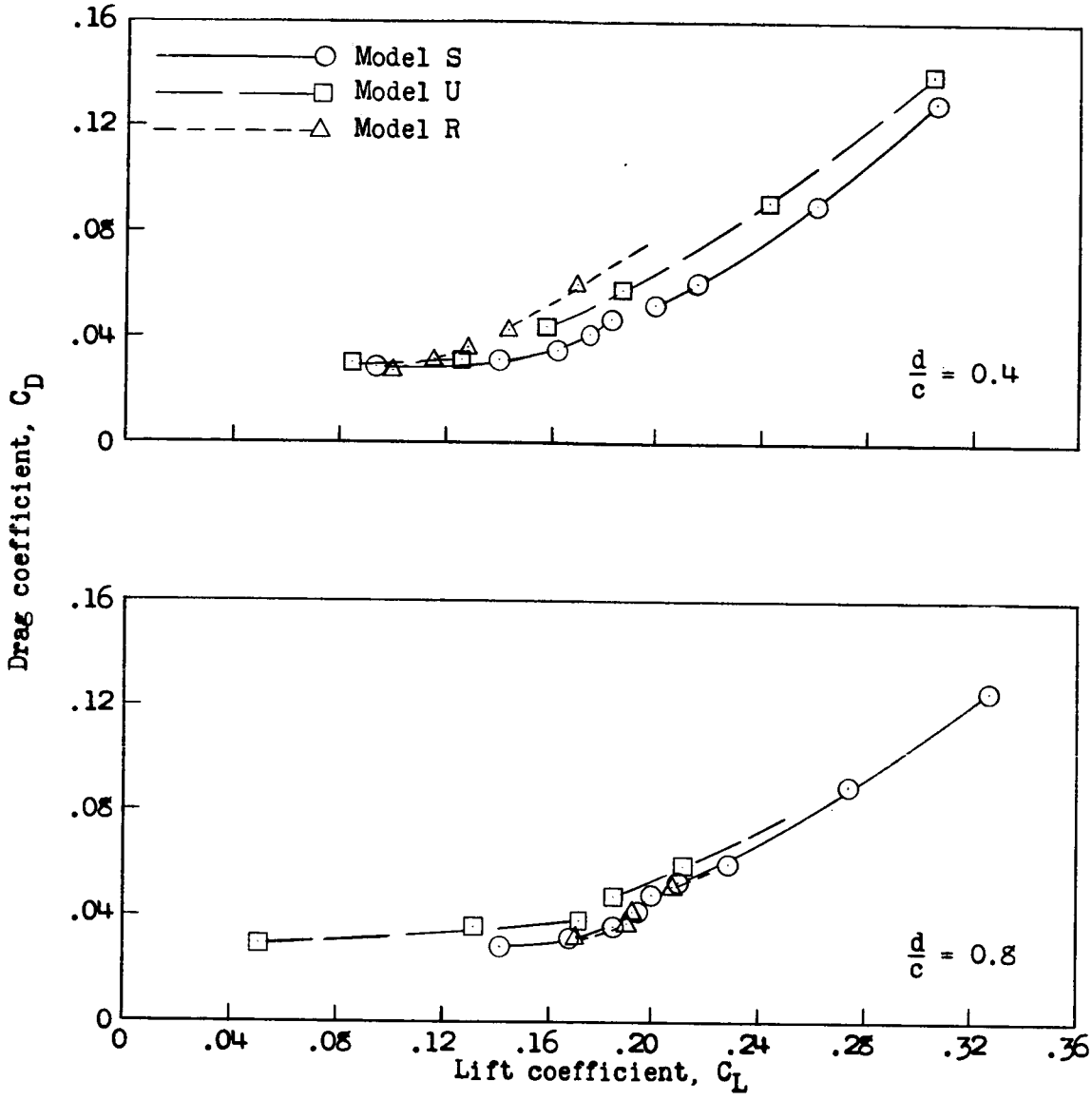

Figure 15.- Variation of drag coefficient with lift coefficient.

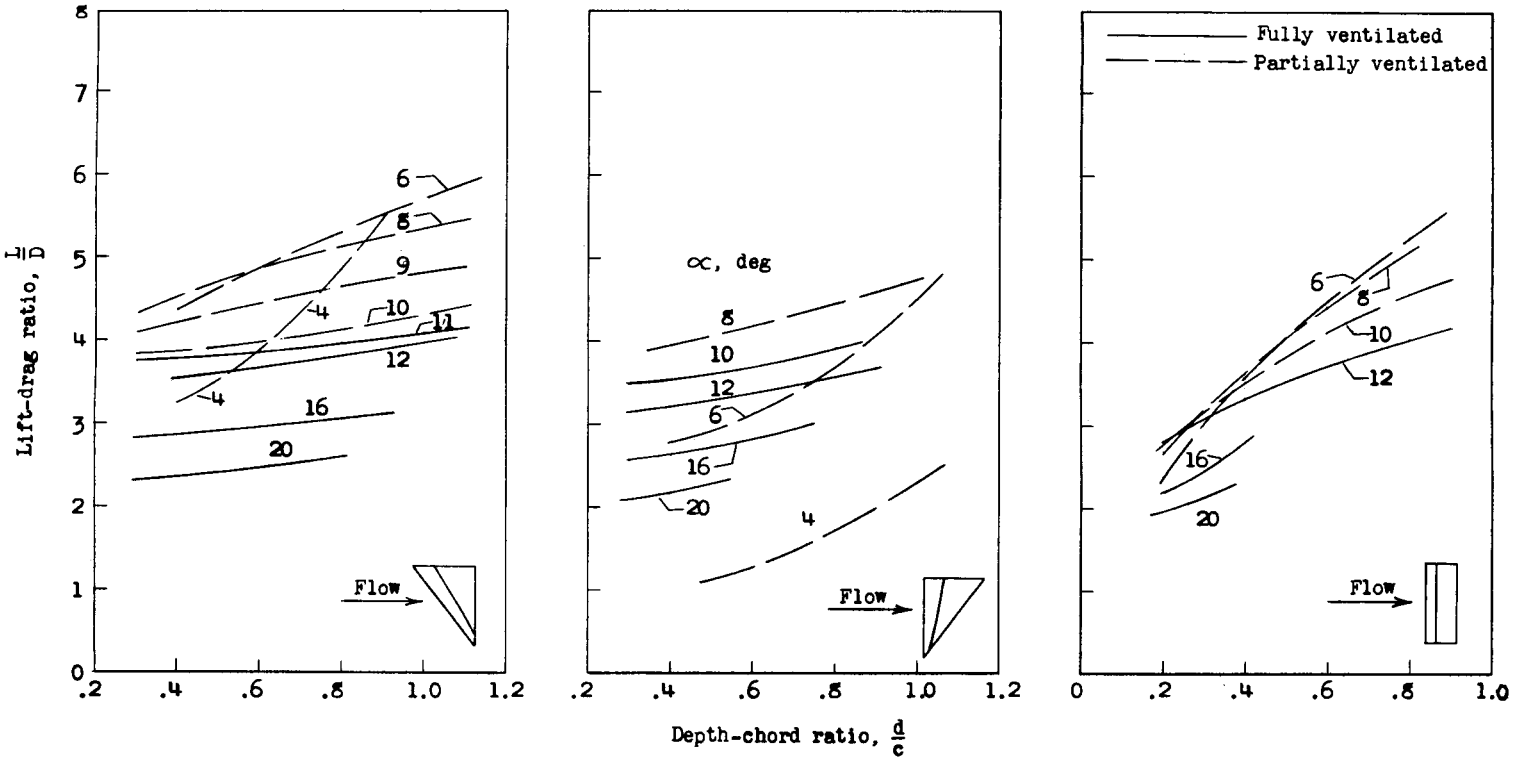

(a) Model S. (b) Model U. (c) Model R.

Figure 16.- Variation of lift-drag ratio with depth of submersion.

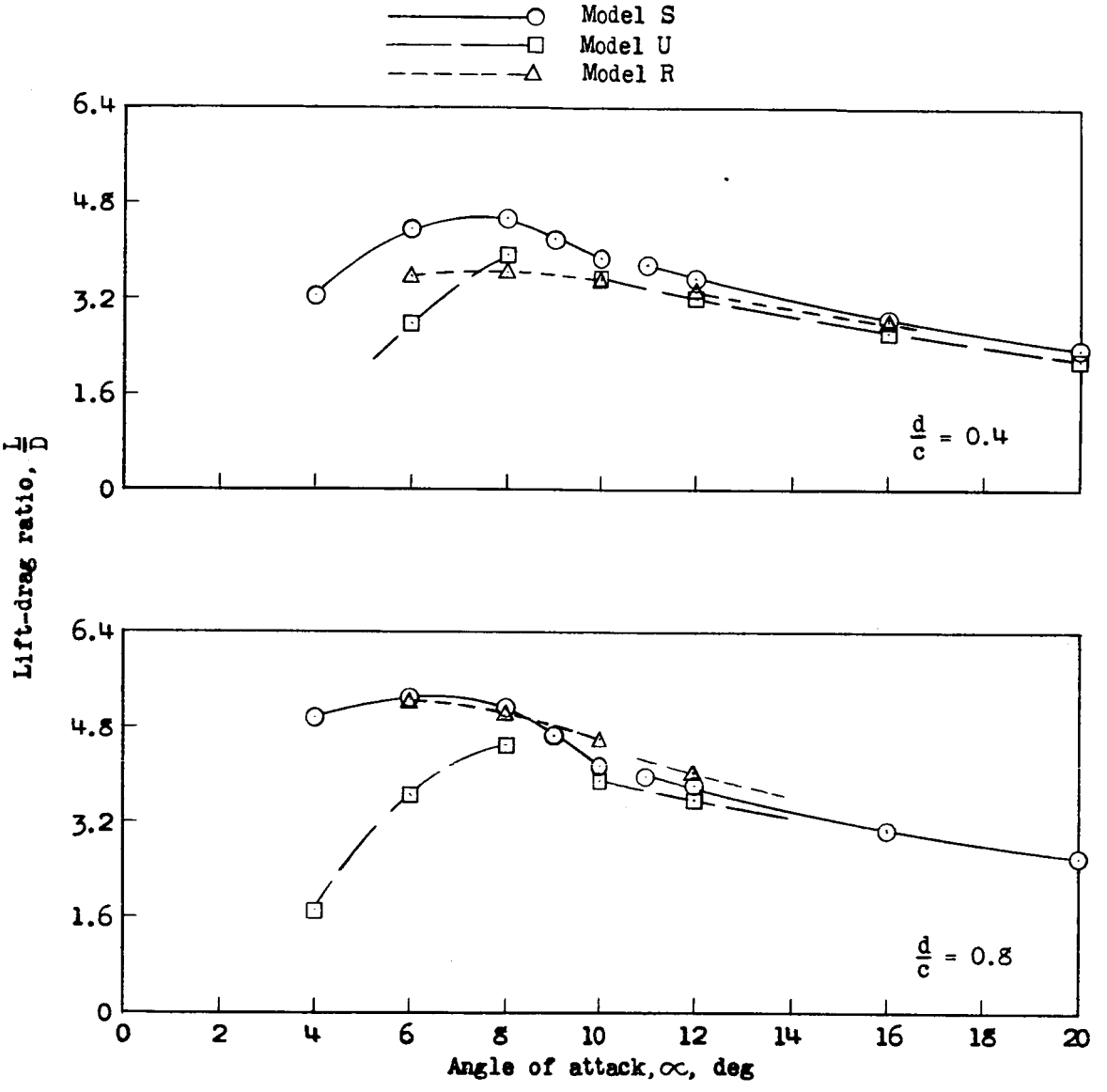

Figure 17.- Variation of lift-drag ratio with angle of attack.

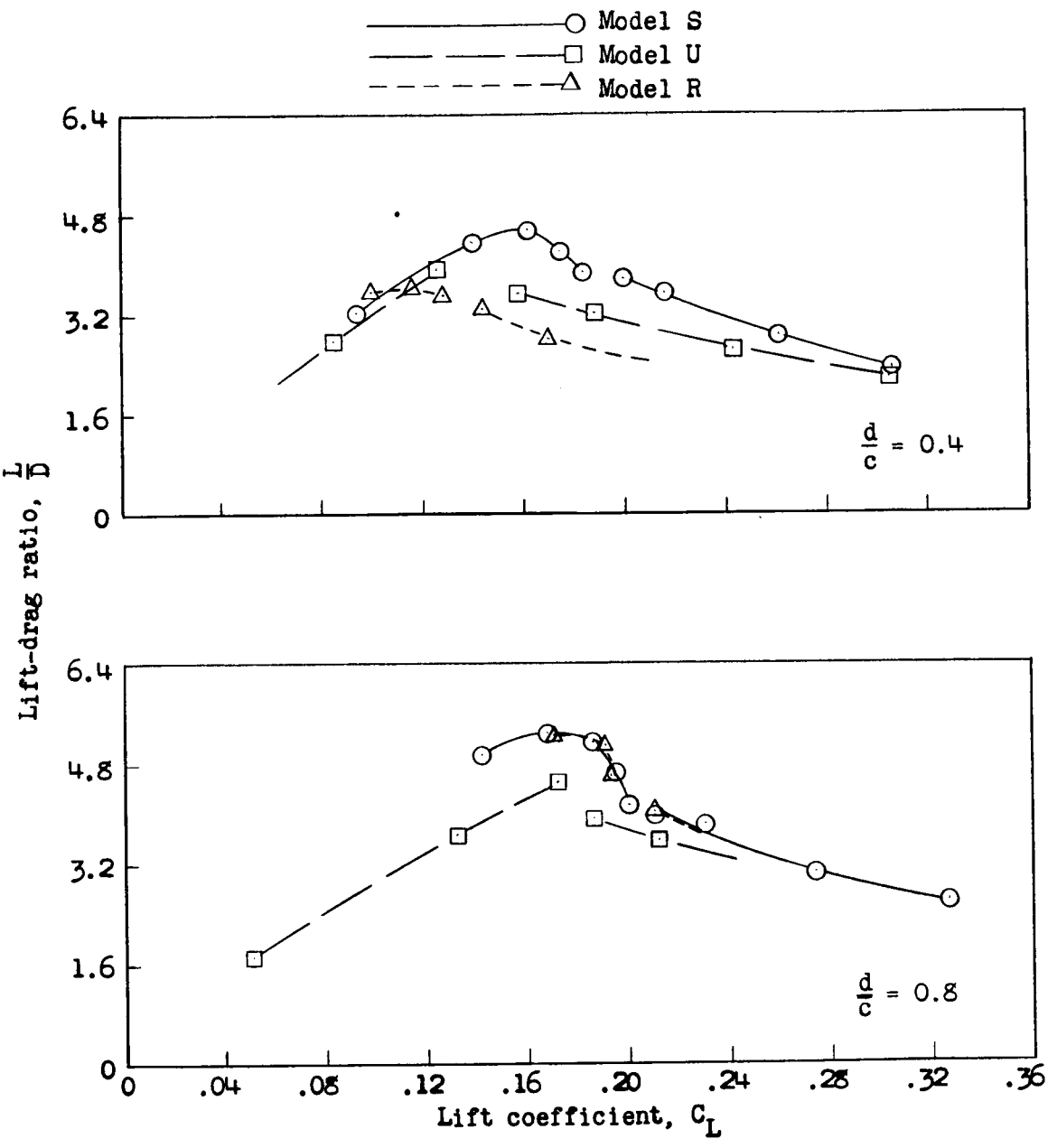

Figure 18.- Variation of lift-drag ratio with lift coefficient.

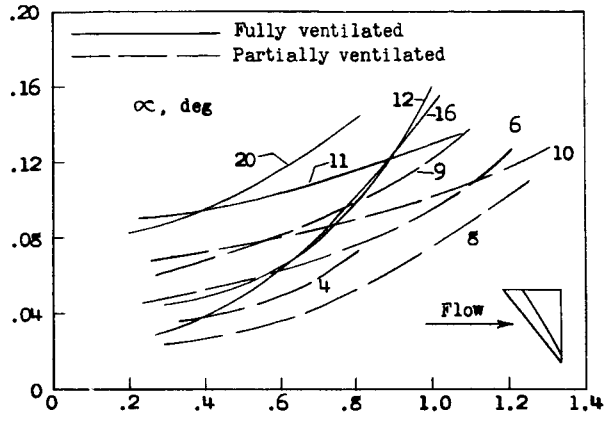

(a) Model S.

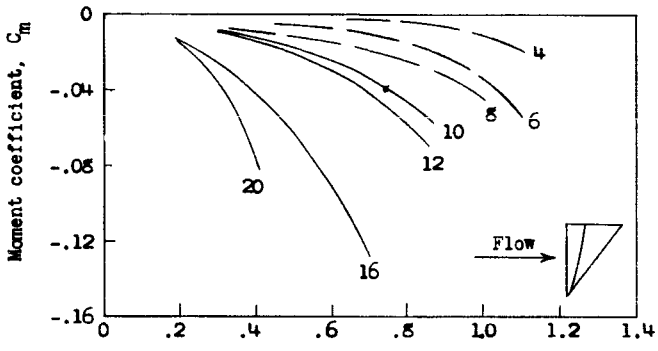

(b) Model U.

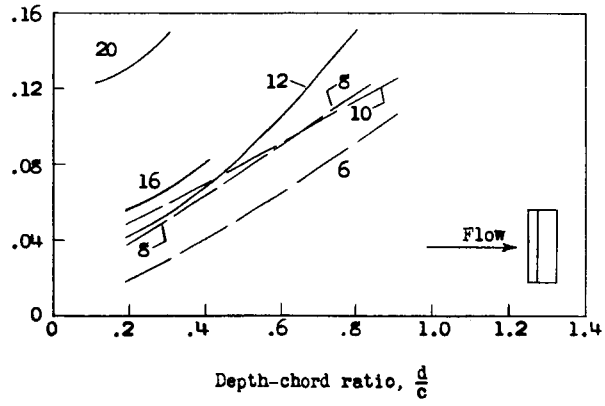

(c) Model R.

Figure 19.- Variation of moment coefficient with depth of submersion.

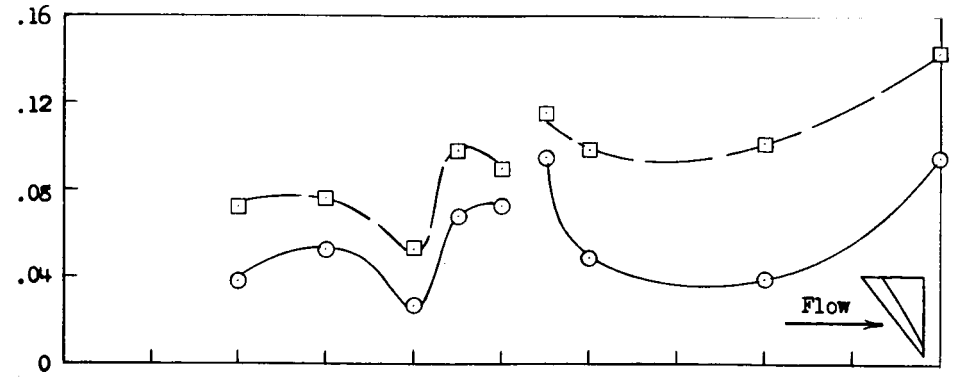

(a) Model S.

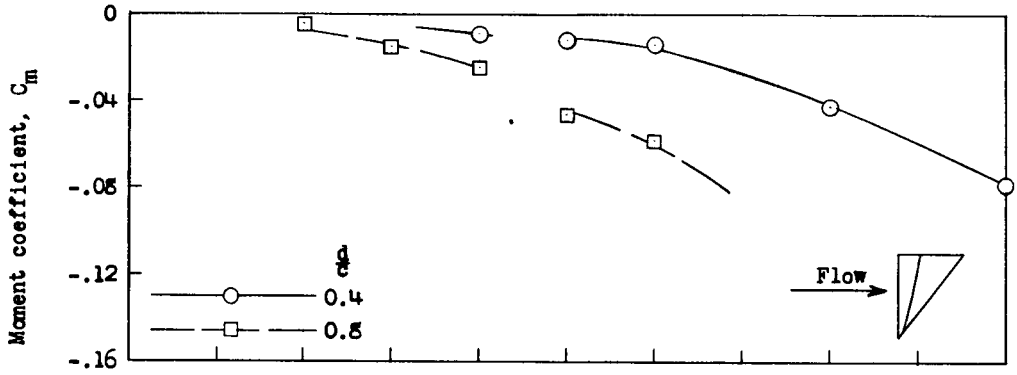

(b) Model U.

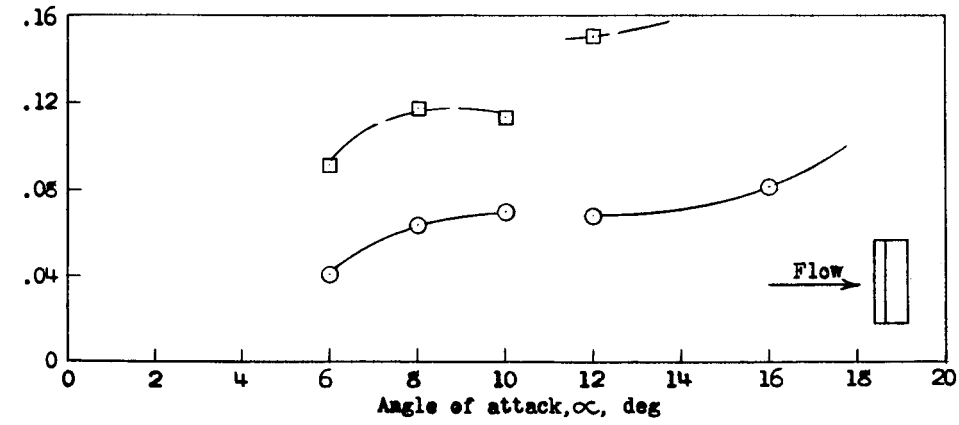

(c) Model R.

Figure 20.- Variation of moment coefficient with angle of attack.

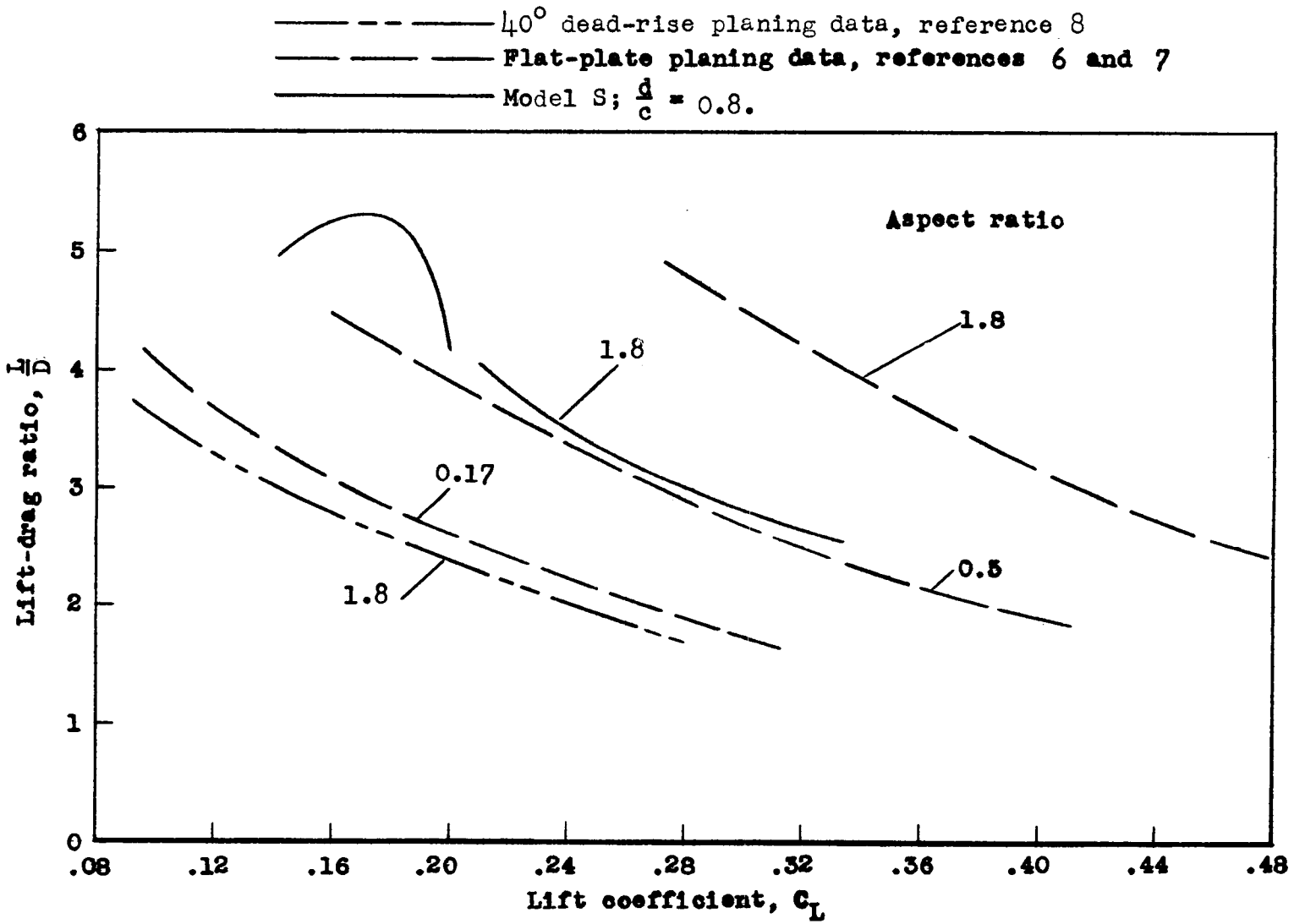

Figure 21.- Comparison of experiment with planing data.

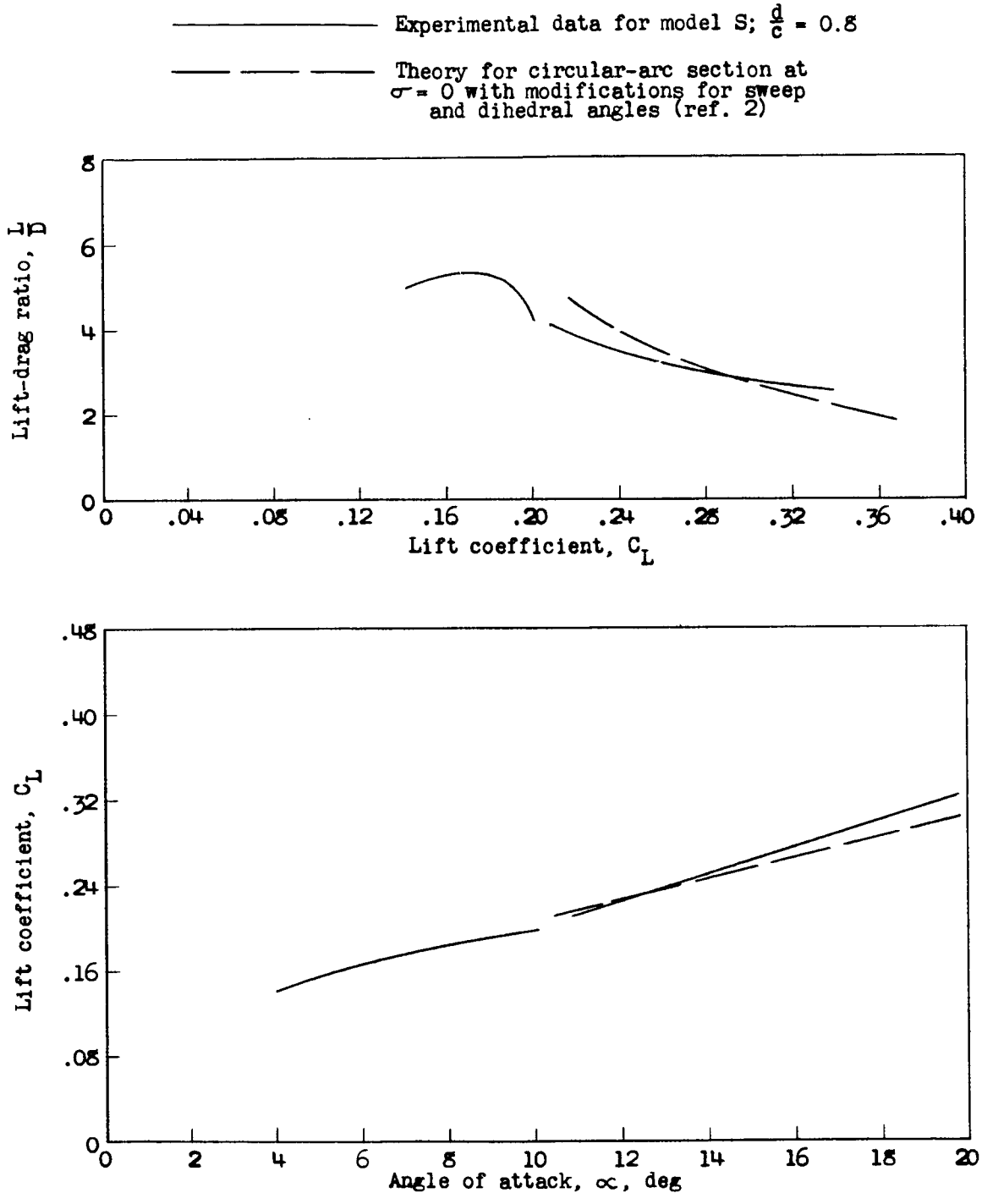

Figure 22.- Comparison of experimental data with theory.

L-313